U.S. Department
of Transportation
National Highway
Traffic Safety
Administration

NHTSA

DOT HS 813 631

October 2025

Parametric Study of Pre-Crash Vehicle Maneuvers and Occupant Safety Performance Response

This page is intentionally left blank.

DISCLAIMER

This publication is distributed by the U.S. Department of Transportation, National Highway Traffic Safety Administration, in the interest of information exchange. The opinions, findings, and conclusions expressed in this publication are those of the authors and not necessarily those of the Department of Transportation or the National Highway Traffic Safety Administration. The United States Government assumes no liability for its contents or use thereof. If trade or manufacturers' names or products are mentioned, it is because they are considered essential to the object of the publication and should not be construed as an endorsement. The United States Government does not endorse products or manufacturers.

NOTE: This report is published in the interest of advancing motor vehicle safety research. While the report may provide results from research or tests using specifically identified motor vehicle models, it is not intended to make conclusions about the safety performance or safety compliance of those motor vehicles, and no such conclusions should be drawn.

Suggested APA Format Citation:

Dahiya, A., Meng, Y., & Untaroiu, C. D. (2025, October). *Parametric study of pre-crash vehicle maneuvers and occupant safety performance response* (Report No. DOT HS 813 631). National Highway Traffic Safety Administration. doi:10.21949/psmm-9151

This page is intentionally left blank.

Technical Report Documentation Page

1. Report No.	2. Government Accession No.	3. Recipient's Catalog No.
DOT HS 813 631		

4. Title and Subtitle	5. Report Date
Parametric Study of Pre-Crash Vehicle Maneuvers and Occupant Safety Performance Response	October 2025
	6. Performing Organization Code

7. Authors	8. Performing Organization Report No.
Akshay Dahiya, Yunzhu Meng, Costin D. Untaroiu	

9. Performing Organization Name and Address	10. Work Unit No. (TRAIS)
Virginia Tech Transportation Institute 3500 Transportation Research Plaza (0536) Blacksburg, VA 24061	11. Contract or Grant No.

12. Sponsoring Agency Name and Address	13. Type of Report and Period Covered
National Highway Traffic Safety Administration 1200 New Jersey Avenue SE Washington, DC 20590	Final Report
	14. Sponsoring Agency Code

15. Supplementary Notes

The contract officer representative for this task order is Dr. Whitney M. Tatem, lead engineer, Vehicle Safety Research, Structures and Restraints.
Digital Object Identifier: https://doi.org/10.21949/psmm-9151

16. Abstract

This report addresses the influence of pre-crash vehicle maneuvers on the injury risks of front passengers during a frontal crash. Seat position and occupant characteristics including anthropometry, sex, and age were also included in the developed design of experiments, which consisted of 55 finite element (FE) crash simulations. A generic buck vehicle model was developed based on a publicly available FE model of a 2014 Honda Accord, which included the vehicle interior and the front passenger air bag (PAB). The PAB model was validated in a drop-tower test, which was designed by the manufacturer, and a reasonable comparison was obtained for oblique side impacts using a Test Device for Human Occupant Restraint-M50, or THOR-M50, in both driver and passenger seats and for frontal impacts using a Hybrid-, or H-, III M50 in the driver seat and H-III F05 in the passenger seat. A generic 1 g braking and turning-and-braking pulse were used as two different pre-crash maneuvers using specific rigid-body human models (Global Human Body Models Consortium [GHBMC] models) with active joints, called the GHBMCsi-pre models. Then, the kinematics data was transferred using a developed switch algorithm to simplified deformable human models (the GHBMCsi models), and a Federal Motor Vehicle Safety Standard No. 208 pulse was applied to simulate the in-crash phase. Injury metrics were recorded for all the belted GHBMCsi models to evaluate injury risks. Seat recline angle and seat track position showed the highest influence on the head injury criteria, or HIC. The brain injury criteria, or BrIC, and neck injury criteria, or Nij, were most sensitive to pre-crash maneuver type, seat recline angle, and occupant model size.

17. Key Words	18. Distribution Statement
pre-crash and in-crash finite element simulations, pre-crash passenger maneuvers, passenger-side air bag, front passenger restraint, seat characteristics, anthropometry, mesh morphing, finite element models, front passenger safety, injury risk assessment, switch algorithm, THOR-M50, GHBMC, FMVSS 208, BrIC, Nij	Document is available to the public from the DOT, BTS, National Transportation Library, Repository & Open Science Access Portal, https://rosap.ntl.bts.gov.

19. Security Classif. (of this report)	20. Security Classif. (of this page)	21. No. of Pages	22. Price
Unclassified	Unclassified	83	

Form DOT F 1700.7 (8-72) Reproduction of completed page authorized

This page is intentionally left blank.

Table of Contents

List of Figures

List of Tables

Executive Summary

The research described in this report was focused on a numerical evaluation of front passengers' injury risks during a frontal crash. Compared to traditional frontal crash simulation approaches, in addition to an in-crash phase, a pre-crash phase was included in the full crash simulation. In addition to pre-crash maneuvers (brake and turn-and-brake), passenger characteristics (anthropometry, sex, age) and seat characteristics (recline/cushion angles, and track position) were considered as variables in the design of experiments. Almost-rigid-body finite element (FE) models with active joints were employed in the pre-crash phase, and then deformable simplified FE models were employed in the in-crash phase.

The main challenges encountered throughout the project's execution that were overcome in partnership with the National Highway Traffic Safety Administration were as follows.

1. *Large computational cost of running long pre-crash simulations*: During a thorough literature review, we found this issue could be resolved by using separate FE models for pre-crash and in-crash phases (Ghosh et al., 2015; Yamada et al., 2016). Global Human Body Models Consortium (GHBMC) models were used in this study. Specifically, a rigid-body GHBMCsi-pre model was used for the pre-crash phase and a deformable simplified GHBMCsi model was used during the in-crash phase.
2. *Accounting for/introduce muscle activation during pre-crash*: The almost-rigid-body pre-crash model (GHBMCsi-pre) was calibrated, in terms of level of joint activation, relative to volunteer test data recorded in pre-crash maneuvers.
3. *Transferring the kinematics of the pre-cash human model at the end of the pre-crash phase to the deformable in-crash human model*: A switch algorithm was developed to ensure successful and efficient position and kinematic transfer to a deformable simplified GHBMCsi (in-crash) model for each of the 55 crash design-of-experiment simulations.
4. *Improving the overall 2014 Honda Accord FE model passenger air bag (PAB) deployment*: In collaboration with researchers from ZF,[1] a robust and symmetric PAB deployment was achieved by making significant changes to the PAB geometry and its interaction with the vehicle interior instrument panel (Singh et al., 2018). A series of PAB validations during frontal and oblique impacts were performed, including a drop tower test to ensure the air bag performance and stability during different crash scenarios.

Report Contents

This report presents the methodologies, results, and analyses associated with the task of using various morphed FE human models to determine how a range of pre-crash occupant kinematics and seat positioning impact front passenger safety. The variables employed in this numerical evaluation are:

- occupant characteristics, including age, body mass index, stature, and sex;
- pre-crash maneuvers, including braking and turn-and-brake; and
- seat positioning parameters, including seat track position and seat recline angle.

The following research components were developed in support of the specific objectives and goals of this study.

[1] The ZF Company; shareholders are the Zeppelin Foundation, administered by the City of Friedrichshafen, Germany (93.8% of shares), and the Dr.-Jürgen-and-Irmgard-Ulderup Foundation, Lemförde, Germany (6.2%).

1. Perform a literature review.
2. Develop a design-of-experiment scheme of pre/in crash FE simulations. Prepare a simplified vehicle buck and a set of morphed GHBMCsi models according to the design-of-experiment scheme.
3. Calibrate the GHBMCsi-pre models against test data related to pre-crash maneuvers and perform design-of-experiment pre-crash simulations.
4. Develop an algorithm for transferring the human body kinematics of the GHBMCsi-pre model to the GHBMCsi model at the start of impact.
5. Prepare, perform, and analyze the results of the GHBMCsi crash simulations.

Section 1 presents the findings of a literature review focused on the influence of integrated crash avoidance and automated driving systems on occupant injury risks. Automatic emergency braking systems influence the occupant's posture and kinematics in both the driver and the front passenger seats. Further, influence of other parameters, such as passenger seat characteristics and anthropometries, are discussed.

Section 2 describes the process to obtain a reduced vehicle model from a mid-sized sedan FE model. Human body model settling and positioning are also discussed briefly. The modified vehicle model is examined for computational efficiency. This section also discusses the GHBMC morphing performed to obtain the in-crash FE models and their positioning.

Section 3 focuses on the pre-crash simulation for two scenarios using 12 different human body models with different anthropometry. Simulations with both active and passive GHBMCsi-pre models are discussed. The use of a CORrelation and Analysis (CORA) score for optimizing the active GHBMCsi-pre models relative to the corridors available from volunteer sled-test data are discussed.

Section 4 covers the details and step process for the switch algorithm where the transfer of data from the pre-crash model (GHBMCsi-pre) to the in-crash model (GHBMCsi) is performed.

Section 5 summarizes the improvements and validation of the PAB model (Singh et al., 2018). The performances of the updated PAB model in the drop-tower test, oblique impacts, and full-frontal impact simulations are discussed.

Section 6 summarizes the design-of-experiment study performed for the crash simulations. Details of the GHBMCsi's positioning and simulation setup are discussed.

Section 7 summarizes the computational results for the performed design-of-experiment study. Injury risks are calculated and analyzed for different scenarios. Inferences are derived based on a sensitivity analysis for the different parameters involved.

Introduction and Scope of Work

Background and Objectives

One of the goals of NHTSA's research initiatives on crash avoidance and automated driving systems (ADSs) is to understand crash safety considerations that are unique to vehicles containing these technologies. Pre-crash maneuvers that may be initiated by a crash avoidance system or ADS generally take up to a few seconds to perform. During this time, heavy braking and/or steering maneuvers may cause occupants to move relative to the vehicle. This motion tends to displace occupants out of the standard driver and passenger postures, which may reduce the effectiveness of current air bag and seat belt systems in the event of a crash (Carlsson & Davidsson, 2011). Further, in ADS-equipped vehicles, occupants may have more choice of how to configure their seats when they do not need to access vehicle controls such as the steering wheel and/or foot pedals, if available. For example, occupants may choose a seat track position that is farther back and/or a larger seat recline angle. Again, this is a unique deviation from what is considered a standard driver posture, for which many current safety systems are designed.

Passenger behavior during two different pre-crash events (brake and turn-and-brake) was investigated under the NHTSA-funded project *Passenger Kinematics During Crash Avoidance Maneuvers* (Reed et al., 2021). Additionally, mostly rigid body models (GHBMC models) with proportional–integral–derivative (PID) joint controllers (called the GHBMCsi-pre models) were developed based on GHBMC simplified models (GHBMCsi) to simulate muscle activation during pre-crash phase (Hu et al., in press). Using a rigid seat model, the GHBMCsi-pre models were used to simulate the pre-crash maneuvers observed in experimental studies.

The overall objective of the proposed research is to evaluate vehicle front passengers' safety using finite element (FE) human body models with various anthropometry, age, and sex while considering (1) occupant kinematics that may be generated from a pre-crash maneuver and (2) occupant seat positioning that may be feasible in an ADS-equipped vehicle. The simulated crash condition is a full-width frontal impact into a rigid barrier at 35 mph (~35 mph (~56 km/h)), as stipulated in the Federal Motor Vehicle Safety Standard (FMVSS) No. 208 test procedure. Another objective was to investigate both the effects of each individual parameter and the combination of parameters on crash outcomes such as occupant kinematics, restraint engagement, and injury measures using a design-of-experiments approach.

Approach

Pre-crash maneuvers may influence an occupant's initial position at the start of a crash phase (Ejima et al., 2009; Stockman, 2016). Coupling the pre-crash phase with the in-crash phase would capture both vehicle and front-passenger kinematics during the full crash simulation. Therefore, the front-passenger simulations performed in the current project consisted of two (2) main phases: a pre-crash phase, and an in-crash phase (Figure 1).

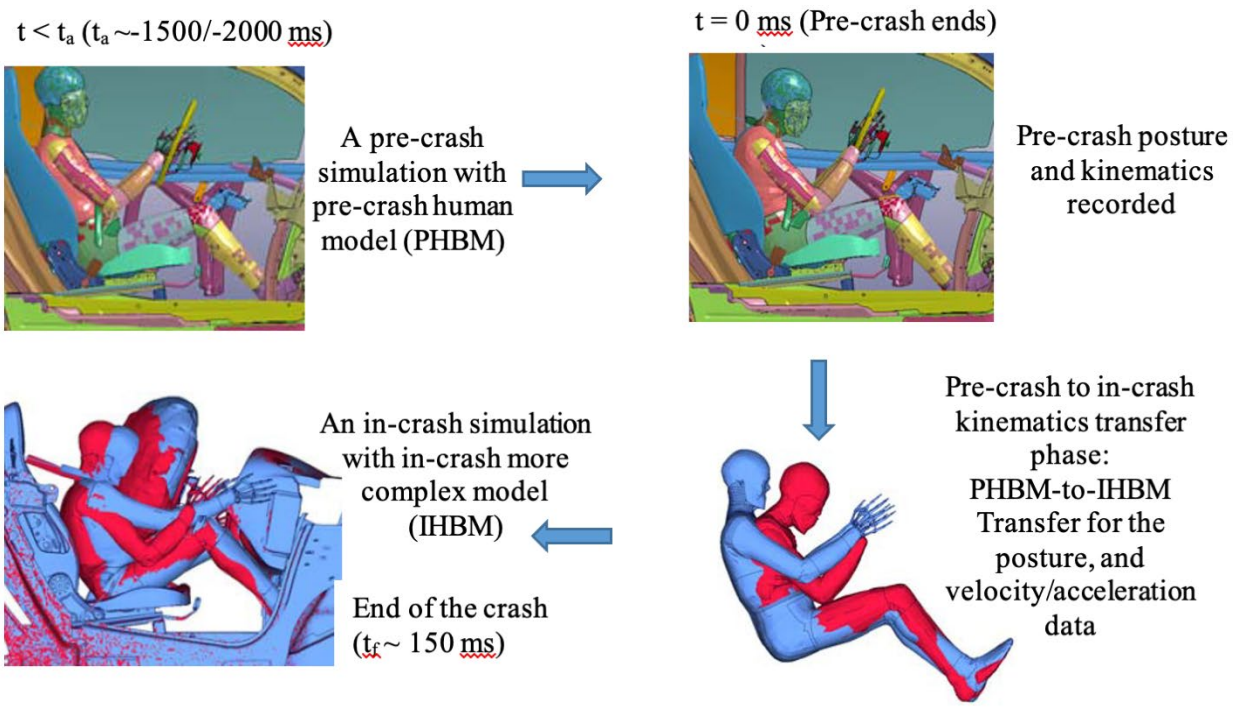

Figure 1. Methodology used to integrate pre-crash vehicle dynamics into occupant injury protection (Ghosh et al., 2015)

1. ***Pre-crash phase***: An almost rigid human body model with the exterior geometry of a GHBMC model and closed-loop muscle activation through PID controllers (GHBMCsi-pre) was used to simulate pre-crash maneuver conditions. To replicate the passenger kinematics during pre-crash maneuvers (e.g., brake and turn-and-brake), these GHBMCsi-pre models (Hu et al., in press) were previously calibrated to volunteer kinematic data before use in the design-of-experiment simulations.
2. ***Data transfer***: The pre-crash kinematics were transferred from a GHBMCsi-pre model to a deformable human body model (GHBMCsi), which showed relatively good injury predictions relative to a GHBMC-O (detailed) model (Schwartz et al., 2015). The transfer was performed at the initiation time of the frontal crash using an in-house switch algorithm based on a segmentation approach. Data transfer from the pre-crash to in-crash phase involved the transfer of human model posture as well as translational and rotational velocities of various human body parts and vehicle parts to introduce pre-crash dynamic effects.
3. ***In-crash phase***: Finally, a frontal crash of 35 mph (~56 km/h) was simulated with the GHBMCsi model and with its initial posture and kinematics data like the GHBMCsi-pre at the end of the pre-crash phase. The passenger's risks of serious injuries (abbreviated injury scale [AIS] 3+) (Gennarelli et al., 2008) were estimated based on head injury criteria (HIC)15, brain injury criteria (BrIC), neck injury (Nij), chest compression, and femur force.

To investigate how a range of passenger anthropometric variations, pre-crash kinematics, and seat positioning impact the front passenger's safety performance response, a reduced factorial design-of-experiments was performed, where the characteristics of the three components

(passenger, seat, and pre-crash maneuvers) were considered as design variables that influenced the results of the simulations (front passenger safety performance).

Literature Review: Pre-Crash Phase

Nearly 50 percent of crashes are preceded by vehicle maneuvering linked to the crash events, such as braking or turning (Ejima et al., 2009; Stockman, 2016). In some circumstances vehicle motion may force people to shift out of their starting positions, potentially into positions where occupant protection systems are less effective in collisions. Current test techniques analyze crash protection for a few extreme "out-of-position" scenarios (Sohr et al., 2007), but most of the testing and restraint optimizations are performed using "in-position" anthropomorphic test devices (ATDs).

The occupants' posture, location, and velocity relative to the car interior and restraint systems change during automatic emergency braking (AEB; Figure 2) (Carlsson & Davidsson, 2011). The amount of muscle contraction was found to be an important component in determining the forward displacement of volunteers subjected to braking pulses (Ejima et al., 2009; Rooij, 2011). It has been reported that a starting posture near the steering wheel can increase the risk of injury for drivers (Bose et al., 2010; Lebarbé et al., 2005) and that driver kinematics during pre-crash can affect occupant interaction with restraint systems and ensuing level of injury (Antona et al., 2011). Because muscular contraction influences occupant position, efforts are being made to incorporate muscular contraction into numerical human body models (HBMs). Meijer et al. (2012) and Osth et al. (2015) successfully simulated occupant kinematic reaction during AEB occurrences using feedback control to manage muscle activation levels in HBMs.

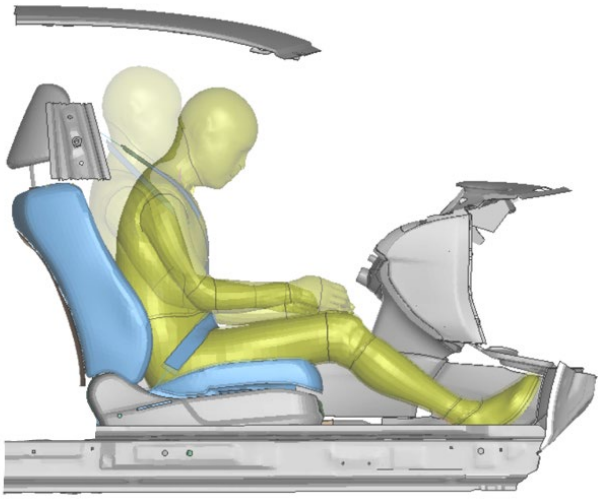

Figure 2. Front passenger posture changes during braking

A classical occupant simulation deals only with the occupant behavior during the crash phase, assuming the human/HBM to be initially in a standard relaxed position. However, vehicle passengers' posture changes due to pre-crash vehicle maneuvers are known to affect their kinematic and injury responses (Carlsson & Davidsson, 2011). It is challenging to study the effect of pre-crash kinematics and posture due to the large computational costs of running a pre-crash simulation using complex FE models that consider muscle activation. Ghosh et al. (2015) presented a simple methodology to integrate pre-crash dynamics into an oblique collision

scenario. The study suggests that a higher driver injury risk is involved when pre-crash braking is considered. The desired positioning for occupant crash simulations involving the Toyota-developed Total Model for Human Safety (Martynenko et al., 2019) was attained via simulations (string-pulling or marionette technique) or geometric transformations (Öztürk et al., 2019).

Yamada et al. (2016) observed that driver injury values decreased when AEB was considered compared to no braking. Lower injury values were credited to forward displacement of the occupant during AEB and reduced impact velocities. The attentiveness of a driver can also be a factor in the positioning of the occupant at the time of the crash and can influence the response of pre-crash braking systems (Rooij, 2011). Activation of pre-braking systems during offset frontal impacts has shown a reduction in impact speeds, which leads to reduced injury risk for vehicle occupants (Infantes et al., 2015).

In this study, to investigate the influence of the passenger's pre-crash maneuvers on the injury response in a frontal crash scenario, computational tools were developed to reduce the computational effort of the pre-crash phase (Ghosh et al., 2015; Öztürk et al., 2019). This work is an attempt to computationally reproduce a full-frontal pre/in-crash and understand how the pre-crash maneuvers influence changes in passenger posture, kinematics, and injury outcome.

FE Vehicle and Human Body Models

To develop a simplified, but accurate, vehicle front buck model, publicly available vehicle FE models were reviewed. At the time of FE vehicle model selection, a total of five sedan models were available to download on the NTHSA vehicle models website (NHTSA, 2020). Three of these vehicle models include interior parts (e.g., dashboard, seat): the 2001 Ford Taurus, the 2010 Toyota Yaris, and the 2014 Honda Accord. These were initially considered as candidates to be used in this study.

A 95th percentile Hybrid III (H-III) ATD model was positioned onto the passenger seat model of the car candidates to investigate if the occupant compartment had enough space to accommodate the ATD model in a standard seating position. It was observed that the 95th male HBM could not fit into the Toyota Yaris or Ford Taurus without changing posture. Considering that an obese human body model (body mass index [BMI]: 40) was to be used in this study, the vehicle with the largest occupant compartment (2014 Honda Accord) and available full restraint model (e.g., seat belt and passenger air bag) was selected to be used in all the simulations.

Development of a Vehicle Simplified Buck Model

The current study involved many design-of-experiment simulations, so it required a significant computational effort. Therefore, two vehicle buck models were developed for this study based on the 2014 Honda Accord FE model.

A generic seat belt model with a shoulder retractor was used for all the simulations (Figure 3a) with the same parameters (e.g., belt pull-in time history Figure 3b) and anchorage locations reported by Hu et al. (in press). The fabric of the seat belt was routed across the occupant model using the LS-PREPOST (LSTC, v. 4.3.14) BeltFit tool.

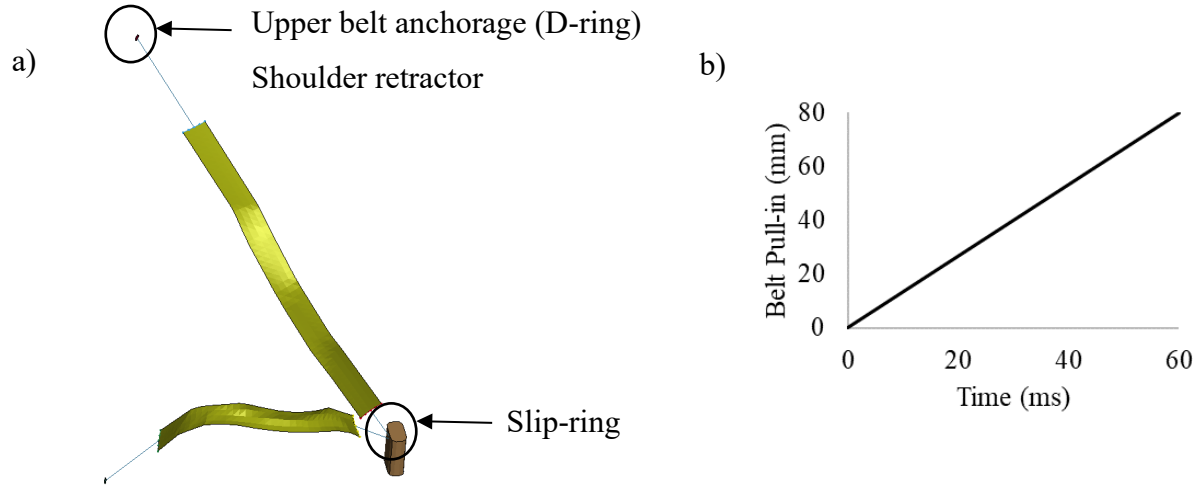

Figure 3. (a) A generic seat belt model with a shoulder retractor and a slip-ring at the buckle; (b) Load curve for belt pull-in vs time after activation

The first vehicle buck had a rigid dashboard and was used for pre-crash simulations with an almost rigid human body model (GHBMCsi-pre). The human body models contacted only a limited number of vehicle parts during the crash simulations, so a simplified buck model would increase computational efficiency while preserving accuracy of results (Figure 4).

To develop this pre-crash buck, the occupant compartment parts of the Honda Accord model were separated. The model consisted of a body-in-white[1] (BIW), dashboard, seat, and carpet parts. In the pre-crash buck model, all the BIW and dashboard parts were changed to rigid. All the BIW parts were constrained to the floor model (Part ID 10001293), and all the dashboard parts were constrained to the main dashboard part (Part ID 16001045) (Figure 4b). The seat frame was also changed to rigid while the seat foam remained deformable, and the bottom frame was used as the reference part (Part ID 50000058) (Figure 4c). The carpet model remained deformable because it was expected to have effects on occupant kinematic behavior (Figure 4d).

In the in-crash buck model figure (Figure 4), the transparent parts used deformable material, while the opaque parts used rigid material. All the other rigid parts were restricted to the red parts, which served as reference objects.

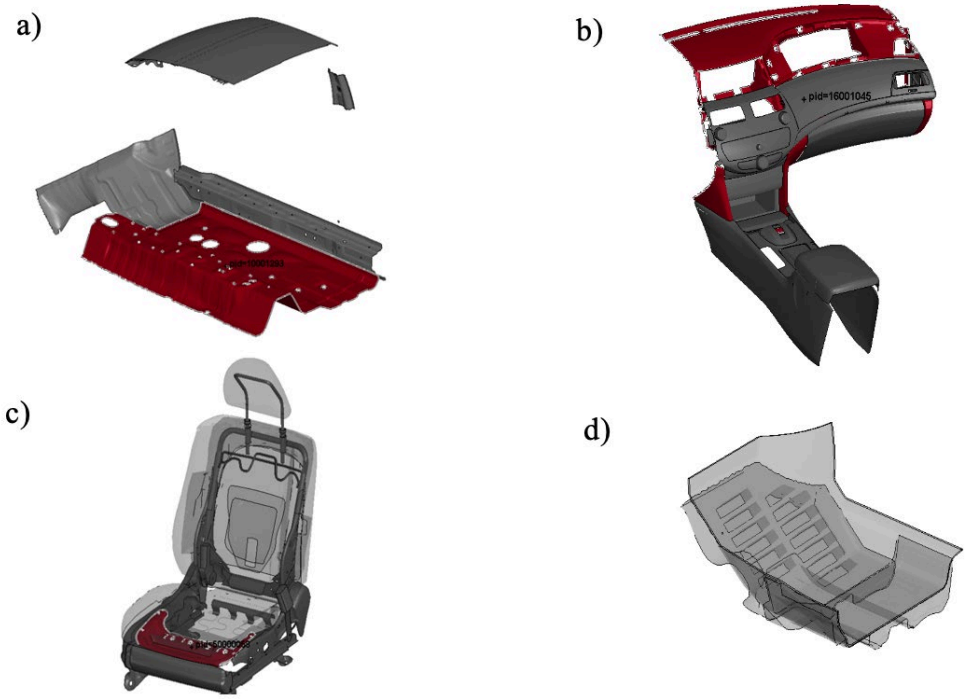

Figure 4. Components of the Honda Accord buck model: (a) BIW; (b) dashboard; (c) seat; (d) carpet

In the second buck, the in-crash buck, the original deformable dashboard was preserved and was used for in-crash simulations with a deformable rigid human body model (GHBMCsi). The BIW, seat, and carpet parts used the in-crash model were the same as the ones used in the pre-crash buck model. Three dashboard parts (Part ID 16001007, 16001043, 16001044) were kept deformable while all the other parts were changed to rigid (Figure 5).

[1] "Body-in-white" is a vehicle manufacturing term for the stage in which a car body's frame has been joined together, but before painting, and before the motor, trim, electronics, and other sub-assemblies have been integrated into the structure.

Figure 5. Dashboard parts used in the in-crash buck model.
Note: Blue parts use deformable material; gray parts use rigid material.

Both the pre-crash buck model and the in-crash model had 307,094 nodes; 593,760 elements; and 96 parts. Detailed information is shown in Table 1.

Table 1. Pre-crash and in-crash buck model information

	Pre-Crash Buck Model	**In-Crash Buck Model**
# of Nodes	307,094	
# of Elements	593,760	
Beam	320	
Shell	298,027	
Solid	295,413	
Rigid	219,722	210,265
Deformable	374,038	383,495
# of Parts	96	96

The LS-DYNA simulation program requires a consistent set of units to be used. Therefore, to couple all parts in one pre-crash simulation, the vehicle and the seat models were converted to GHBMC metric units.

Mass scaling was employed in the buck model to increase computational efficiency. The original Honda Accord full-size vehicle model used a time step of $7*10^{-7}$ s, while in the simplified buck, a time step 10 times higher was used. A comparison was then made between the simulations with different mass scaling values to investigate the model stability and reduction of computational time. To simulate the passenger's effect, an 80 kg rigid plate impactor was used to impact the seat foam during crash simulations. An initial velocity of -1 m/s was assigned to the rigid impactor to ensure that contact between the impactor and seat foam would occur. A constraint was assigned to all the rigid parts such that only translation along the x-axis was allowed. Then, appropriate crash pulses for pre-crash and in-crash phases were assigned to the simplified buck models. Each crash phase was simulated with a time step of $7*10^{-7}$ s and of $7*10^{-6}$ s. All four

simulations were successfully completed, and the CPU time and clock time taken to complete the simulation were also recorded. As seen in Table 2, the simulation times for both in-crash and pre-crash phase were reduced more than 34 times with a time step of $7*10^{-6}$ s than with a time step of $7*10^{-7}$ s.

Table 2. CPU time and clock time for pre-crash seat model and in-crash seat model struck by plate impactor

	Pre-Crash Seat Model	In-Crash Seat Model	Difference
CPU Time	135.33 hours	118.48 hours	12%
Clock Time	3.91 hours	3.42 hours	13%

Development of a Set of Simplified Human Models (GHBMCsi) With Various Anthropometric Characteristics

A set of pre-crash models (Hu et al., in press) consisting of 12 mostly rigid body active models (GHBMCsi-pre; Figure 6) were available to replicate overall occupant kinematics during the pre-crash phase. To evaluate the front passenger's injury risk, the overall kinematics of the GHBMCsi-pre models had to be transferred to deformable HBMs with the same anthropometric characteristics before simulating the in-crash phase. The GHBMCsi simplified model was chosen as a typical deformable HBM to be used in these in-crash simulations due to its computational efficiency and its reasonable predictions relative to detailed GHBMC models (Schwartz et al., 2015). Therefore, a set of in-crash GHBMCsi models that matched the GHBMCsi-pre models' anthropometry were developed using a morphing approach.

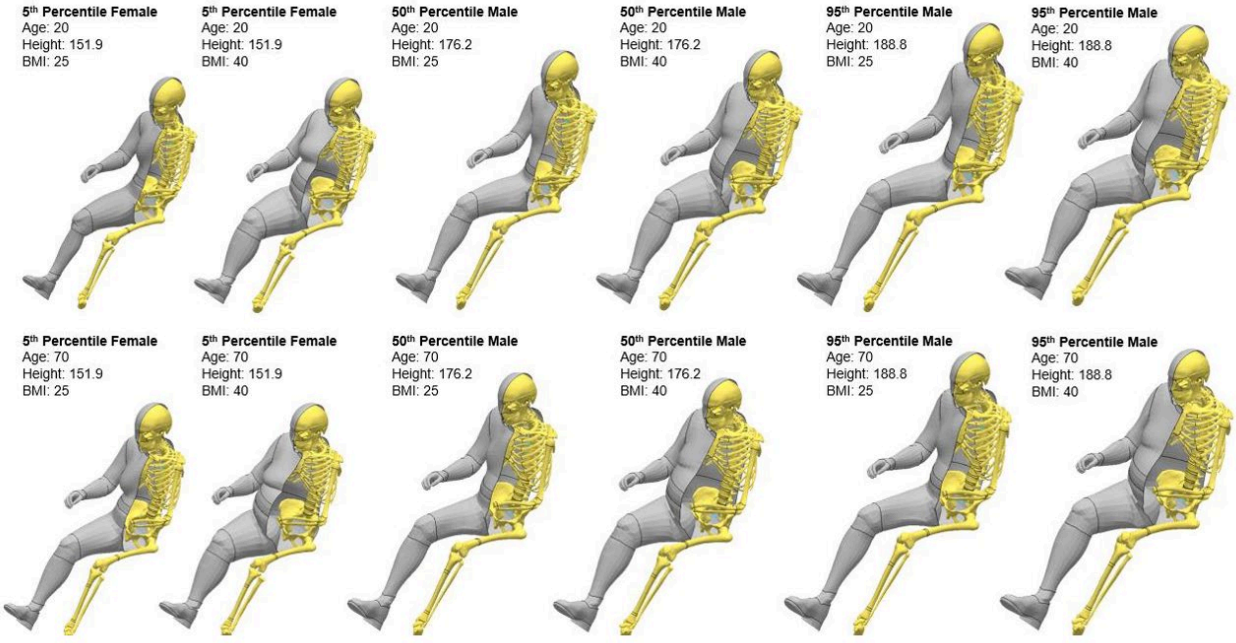

Figure 6. A set of 12 almost rigid body active models (GHBMCsi-pre) used in the FE simulations the pre-crash phase

In the development process of the in-crash models (Figure 7), a library of morphed GHBMCsi models, containing 50 male and 50 female HBMs with various anthropometrics/age, was used. For each target GHBMCsi-pre model, an HBM from that library close to its overall stature and BMI was identified. Then, the identified model was morphed in two phases: (1) the chosen GHBMCsi was positioned to the position of the GHBMCsi-pre at the end of the pre-crash phase and (2) the GHBMCsi was morphed to the exterior geometry of the GHBMCsi-pre target model using HyperMorph Module.[2] Finally, the element quality of the morphed model was checked and improved if necessary. Overall, the final mesh quality (aspect ratio, minimum angle, maximum angle, etc.) of morphed HBMs showed to be in good agreement with corresponding data of the original GHBMCsi model. The overall mass of the morphed GHBMCsi model was also adjusted to match the target by slightly adjusting the flesh density.

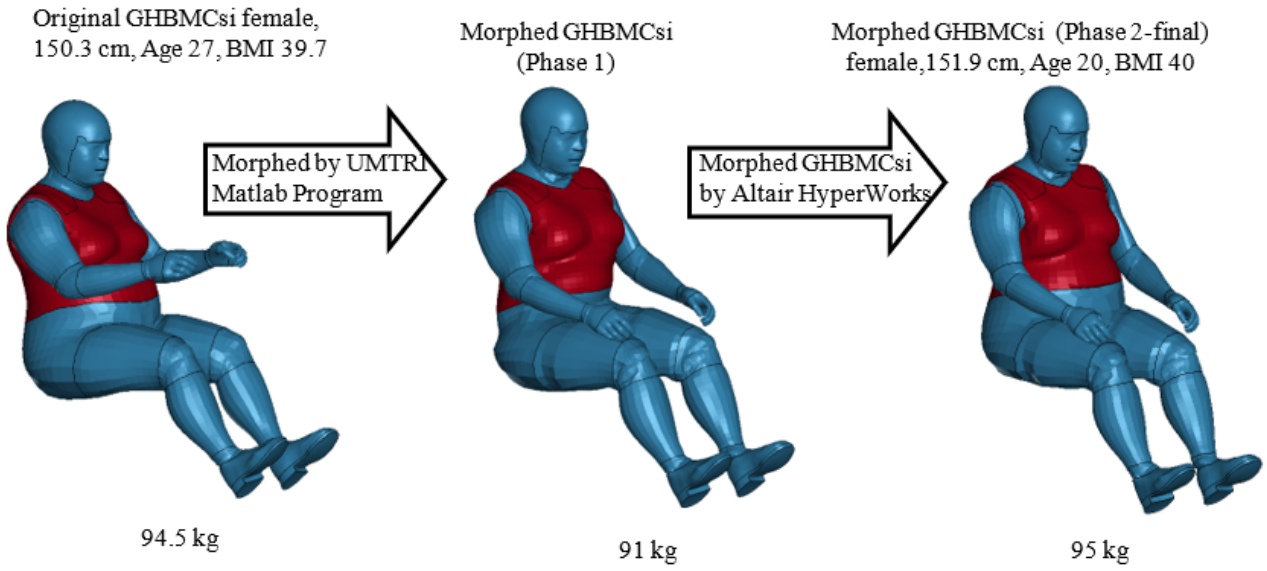

Figure 7. Morphing procedure for a 5th percentile female (age 20, BMI = 40)

[2] Altair Engineering Inc, Troy, MI

This page is intentionally left blank.

Pre-Crash FE Simulations

Pre-Crash Model Versus In-Crash Model

NHTSA previously funded an experimental project (Reed et al., 2021) to record and investigate front passenger kinematics during brake and turn-and-brake pre-crash scenarios. Results demonstrated that pre-crash maneuvers can produce a range of occupant postures, many of which would be considered "out of position" in a crash scenario. Under an additional project (Hu et al., 2019), the pre-crash experimental data was used to develop a mostly rigid body model GHBMCsi-pre (Figure8) based on a GHBMC simplified (deformable) model (GHBMCsi Figure 9). The GHBMCsi-pre model is a modified GHBMCsi model.

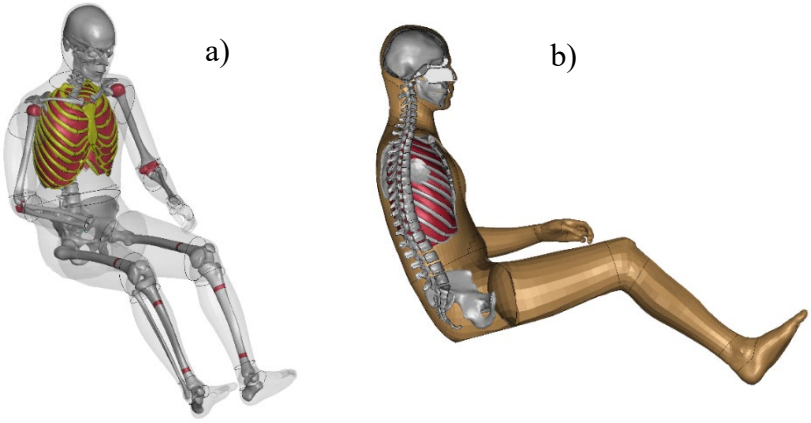

Figure 8. GHBMCsi-pre M50 geometry and basic mesh. (a) thoraco-abdominal geometry, and skeletal structure geometry, (b) lateral view – mid cross-section

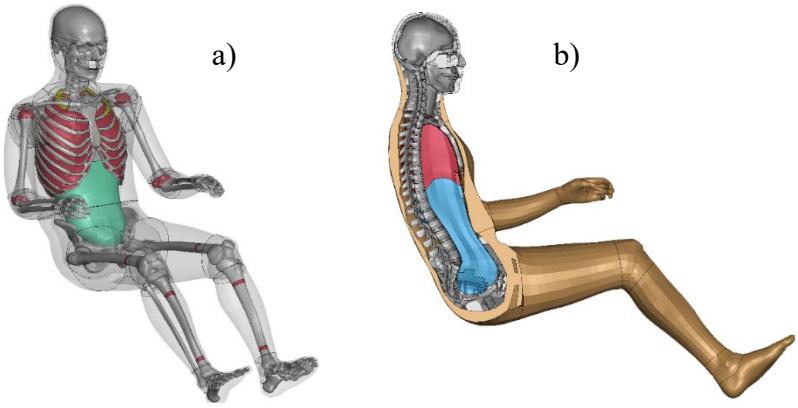

Figure 9. GHBMC M50-OS v1.8.4 geometry and basic mesh. (a) thoraco-abdominal geometry, and skeletal structure geometry, (b) lateral view – mid cross-section

Most of the GHBMCsi simplified model's parts were defined as deformable (363 of 535), including the flesh parts, and has all joints defined in LS-Dyna (Figure 9). On the other hand, the mostly rigid pre-crash model (GHBMCsi-pre) had many of its parts (63%) defined as rigid (including its skin) and no flesh parts (Figure 8). A summary of the two models is provided in Table 3.

Table 3. GHBMCsi and GHBMCsi-pre model summary (without shoes)

	GHBMC M50-OS (v1.8.4)		GHBMCsi-pre	
Number of Parts:	535	Rigid: 172	334	Rigid: 210
		Deformable: 363		Deformable: 124
#Elements:	353,149		265,775	
#Nodes:	290,190		210,684	
Mass (kg):	78.5		76.7	

While GHBMC M50-OS is a passive model (no muscle activation), the GHBMCsi-pre model incorporates a series of PID controllers (Figure 10) to the cervical and lumbar spine joints to simulate the active muscle effects during pre-crash maneuvers (Table 4). These PID controllers can be actuated through a set of PID coefficients, known as controller gains (Table 5). During the pre-crash simulations, the active GHBMCsi-pre used 12 customized controller gains to control the whole-body responses. The 12 controller gains can be grouped into four different sets, and each set controlled the motion of spinal joints in a single direction (fore-aft or lateral).

Table 4. Functionality of 12 customized controller gains

Parameter	Controller Gain Description	Control Joints	Control Direction
kp_Ls	Proportional Gain	Lumbar Joints	Fore-aft Excursion
ki_Ls	Integral Gain		
kd_Ls	Derivative Gain		
Lkp_ Ls	Proportional Gain	Lumbar Joints	Lateral Excursion
Lki_ Ls	Integral Gain		
Lkd_ Ls	Derivative Gain		
kp_Cs	Proportional Gain	Cervical Joints	Fore-aft Excursion
ki_Cs	Integral Gain		
kd_Cs	Derivative Gain		
Lkp_ Cs	Proportional Gain	Cervical Joints	Lateral Excursion
Lki_ Cs	Integral Gain		
Lkd_ Cs	Derivative Gain		

If all controller gains were set to zero, GHBMCsi-pre responded passively. The joint PID control was activated when the value of any controller gain was changed, producing specific model responses. GHBMCsi-pre had the same defined joints as GHBMCsi (e.g., shoulder, elbow, knee, hip), but only Lumbar Spine (LS) Joints and Cervical Spine (CS) Joints' responses were controlled using PIDs.

Table 5. Effect and range of the PID parameters

Parameter	Value	Effect
switch	0	Disengage active joint controllers
	1	Engage active joint controllers
act_lvl	0 to 15	Covers the majority of occupant kinematics
	15 to 40	Covers stronger muscle activations

Two parameters, "switch" and "act_lvl," were used to control the active joints (Table 0-3). "Switch" determined whether active joint controllers would be activated or not, while "act_lvl" controlled the level of muscle activation with a range from 0 to 40.

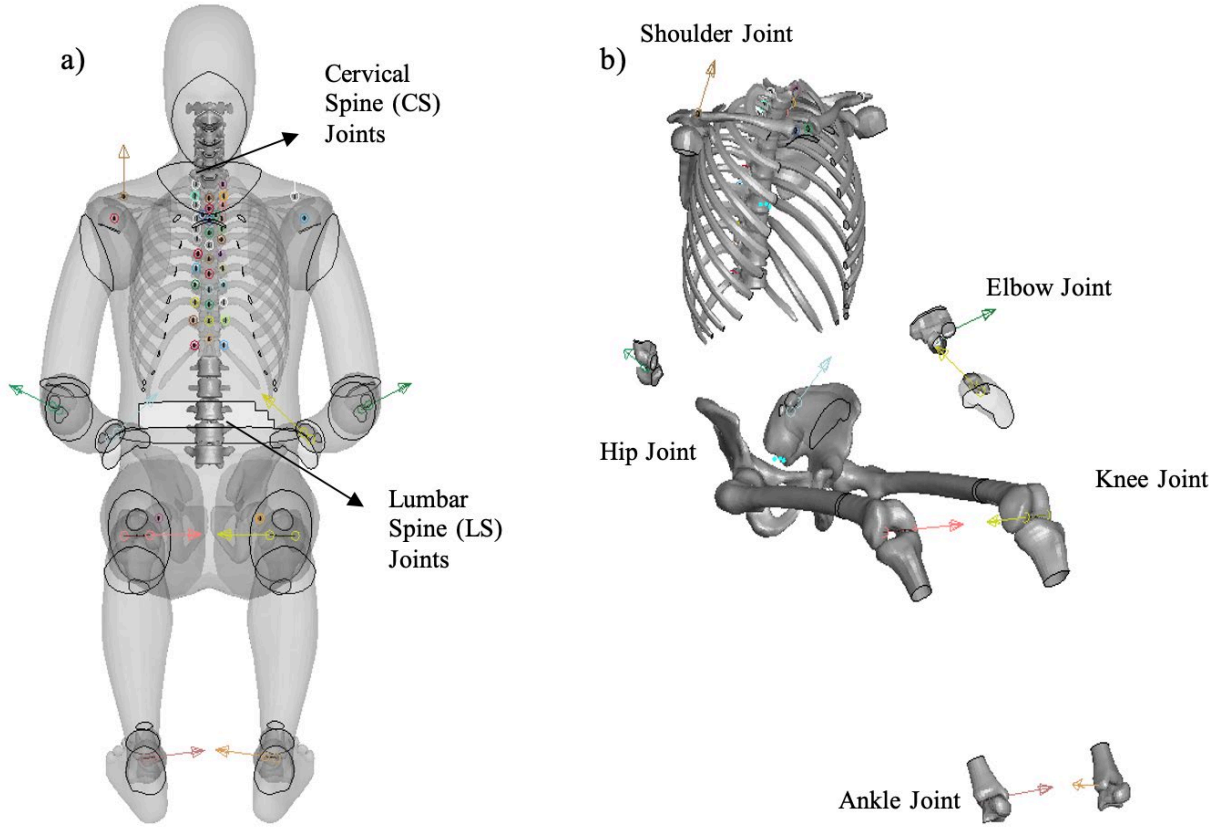

Figure 10. (a) PID controllers used at lumbar spine (LS) joints and cervical spine (CS) joints, (b). Shoulder, elbow, knee, hip, and ankle joints also defined in GHBMCsi-pre.

Pre-Crash Simulations With the Passive GHBMCsi-pre Model

Several preliminary simulations were conducted using the GHBMCsi-pre model (M50, BMI: 25) under abrupt brake and turn-and-brake maneuvers. These pre-crash simulations were performed in two test setups (Figure 11): (a) using the simplified buck based on the developed 2014 Honda Accord FE model and (b) using a rigid seat test setup (Hu et al., 2019).

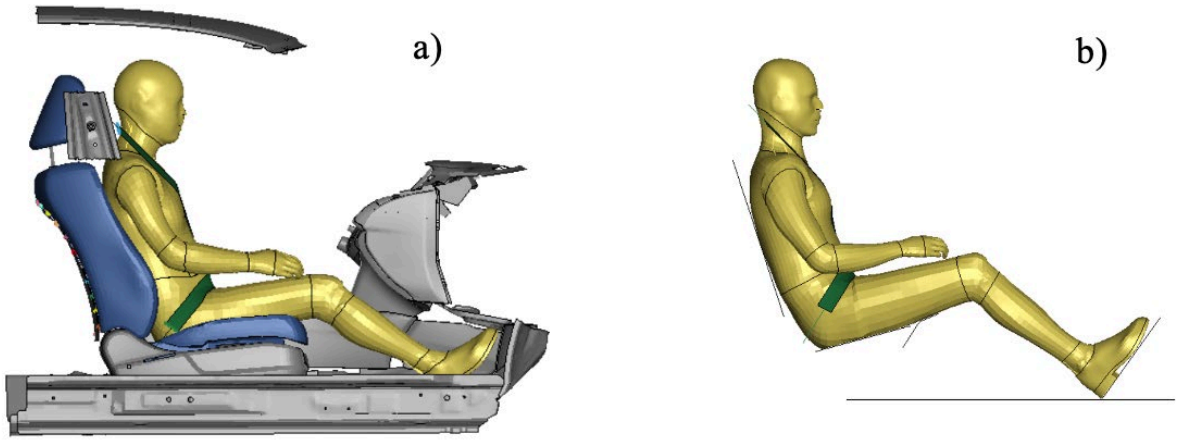

Figure 11. The pre-crash simulation test setups (a) simplified vehicle buck; (b) rigid test setup

The time history of the vehicle accelerations during the pre-crash brake phase was used as input (Figure 12a). The GHBMC head excursions were then measured and compared to the previously published corridors (Hu et al., in press; Figure 12b). In the abrupt brake event simulation, the head excursions showed agreement to the ones recorded from the rigid seat model for the first 300 ms, while a lower excursion was observed overall (Figure 12b). This suggested that the GHBMCsi-pre models in the deformable 2014 Honda Accord buck model should be recalibrated by changing the parameters of active joints to provide accurate predictions against test data corridors.

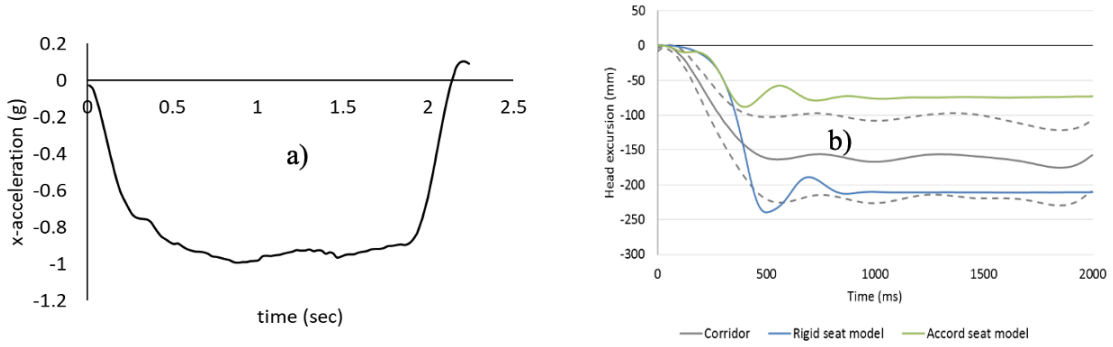

Figure 12. Abrupt brake event time histories of (a) vehicle acceleration and (b) head excursion

In the brake-and-turn event simulation, it was observed that the size of the vehicle center console affected the occupant head excursions. Therefore, an extra center console model, which was the same as the one used in the rigid seat model, was added to the Accord buck model (Figure 13).

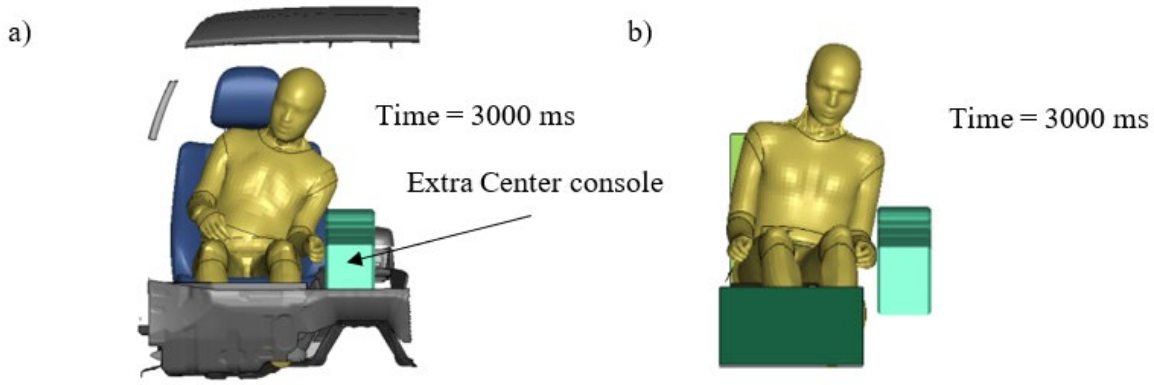

Figure 13. Front passenger behavior during turn-and-brake event simulation (front view): (a) Accord seat model; (b) rigid seat model

The time history of the vehicle accelerations during the pre-crash turn-and-brake phase was used as input (Figure 14a). The simulation results were then reviewed to ensure they were comparable to the ones recorded from the rigid seat simulations. The head excursions (both longitudinal and lateral) of the passive GHBMCsi-pre model were observed to be like the ones recorded in the simulations with the rigid seat model (Figure 14b, (c). The lateral head excursion was observed to be larger than the corridors. Therefore, as in the abrupt brake case, additional calibration of active joints was performed to correlate the results of the simulations with the deformable seat to the test corridor data.

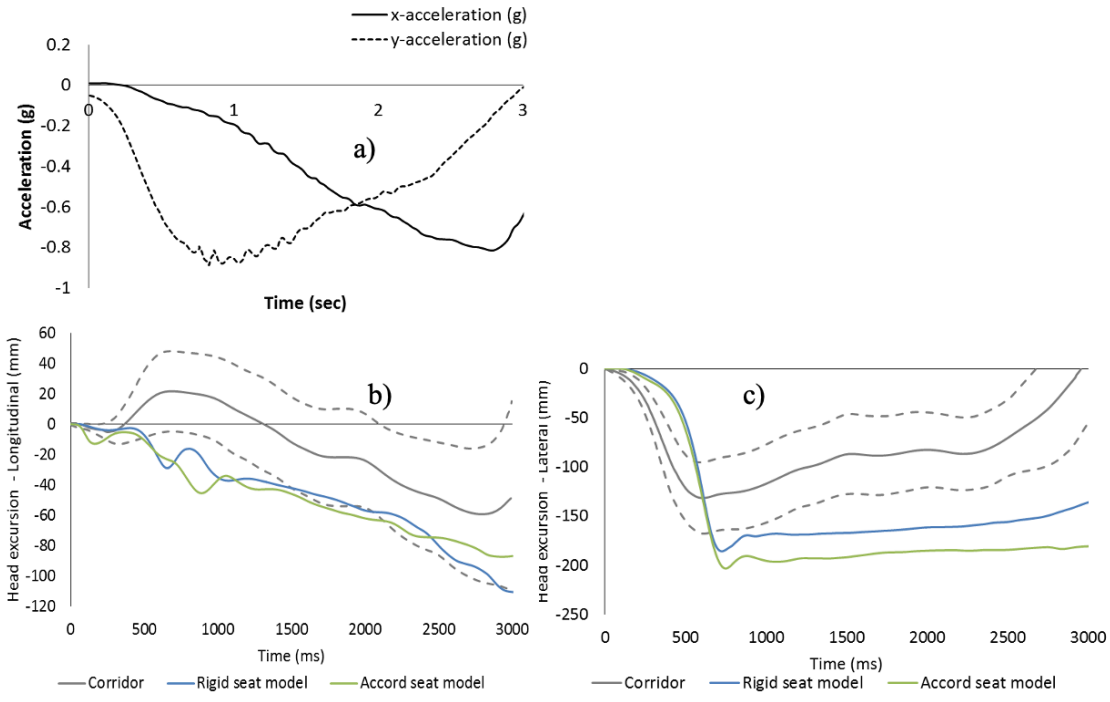

Figure 14. Turn-and-brake event time histories of (a) vehicle acceleration – occupant head excursion, (b) longitudinal head excursion, and (c) lateral head excursion

Pre-Crash Simulations With the Active GHBMCsi-pre Model

To find the simulations which showed the best agreements to the previously published corridors (Hu et al., in press), the GHBMCsi-pre models with multiple active levels were used in the pre-crash simulations. The maximum head excursion decreased with increasing active levels (a typical example based on the M50 model [Age: 20, BMI: 25] is shown in Figure 15).

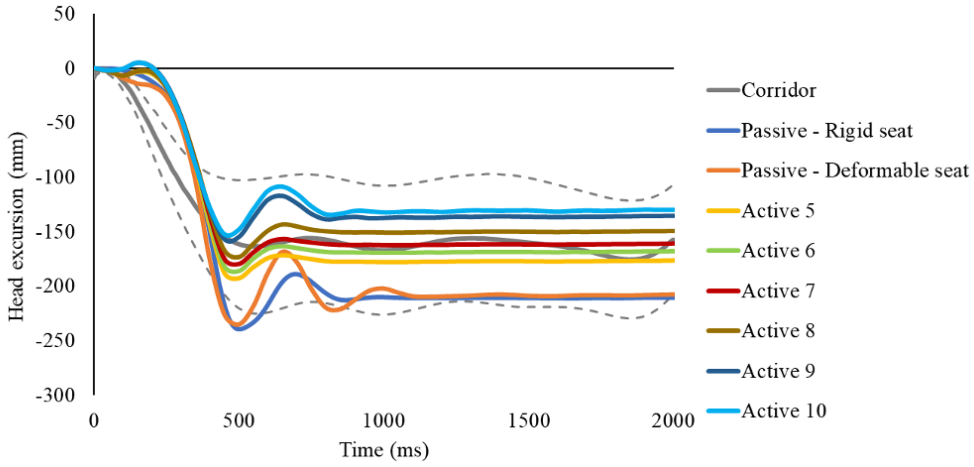

Figure 15. Head excursion of passive and active GHBMCsi-pre (Model No. 5) models in pre-crash simulations

CORA scores were calculated for each activation level to evaluate the agreement between the simulation results and the corridors to choose the most appropriate activation level. Overall, the CORA scores of the final models were good (0.76–0.99; Table 6). The average CORA scores were 0.967 and 0.863 for the abrupt brake and the turn-and-brake events, respectively. It should be mentioned that the corridors for the abrupt brake events varied depending on age and BMI, while all the turn-and-brake simulations were compared to the same corridor (Hu et al., 2019). This may have been the cause of the lower CORA scores in the turn-and-brake event simulations relative to the brake event simulations.

Table 6. CORA scores for head excursion curves

GHBMC Information				Abrupt Brake		Turn-and-Brake	
Model No.	**Size**	**Age**	**BMI**	**Active Level**	**CORA**	**Active Level**	**CORA**
1	F05	20	25	AL0	0.984	AL4	0.781
2	F05	20	40	AL3	0.97	AL0	0.798
3	F05	70	25	AL5	0.955	AL8	0.848
4	F05	70	40	AL9	0.947	AL0	0.759
5	M50	20	25	AL7	0.975	AL11	0.836
6	M50	20	40	AL7	0.99	AL5	0.882
7	M50	70	25	AL10	0.976	AL14	0.886
8	M50	70	40	AL17	0.967	AL15	0.923
9	M95	20	25	AL4	0.98	AL7	0.887
10	M95	20	40	AL9	0.985	AL17	0.896
11	M95	70	25	AL10	0.943	AL18	0.915
12	M95	70	40	AL35	0.929	AL6	0.943
Average CORA Score Throughout the 12 Models							
				Brake		**Turn-and-Brake**	
		Average CORA		**0.967**		**0.863**	

Switch Algorithm: Transfer From Pre-Crash to In-Crash

One of the challenging tasks of this research was to reduce the computational cost of long pre-crash simulations. As established in earlier sections, this issue was resolved by using separate FE models for pre-crash (GHBMCsi-pre) and in-crash (GHBMCsi) phases. A switch algorithm used a segmentation approach for transferring pre-crash kinematics from the GHBMCsi-pre model at the end of the pre-crash simulation to the GHBMCsi kinematics at the beginning of the in-crash simulation (t = 0). This kinematics transfer included the posture and velocity/acceleration of human body model parts.

The GHBMCsi-pre-predicted pre-crash occupant postures served as the input for the GHBMC v1.8.4.1 (GHBMCsi) positioning for crash simulations. Figure 16 shows a flow chart for morphing/post-processing of the GHBMCsi-pre model output to prepare the in-crash GHBMCsi, which included the data transfer from pre-crash to in-crash.

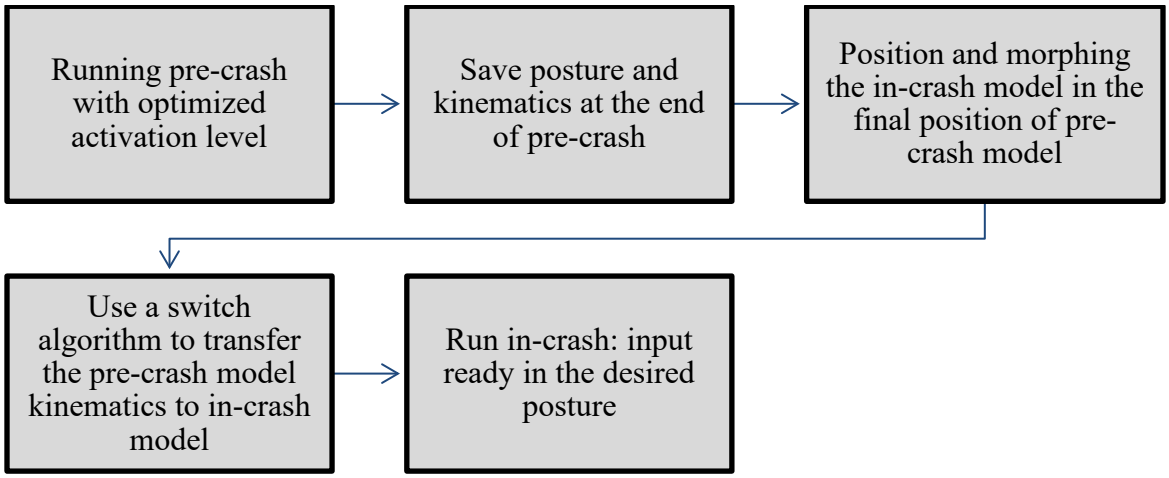

Figure 16. Flow chart for morphing/post-processing of the GHBMCsi-pre simulation to prepare in-crash GHBMCsi simulations

Running Pre-Crash With Optimized Activation Level

In this step, two pre-crash scenarios for each model were considered: (a) abrupt brake and (b) turn-and-brake maneuvers. The activation levels of each pre-crash model were determined based on the highest CORA scores relative to the corresponding test corridors. More information can be found in the previous section (Section 3).

Save Posture and Kinematics at the End of Pre-Crash

The posture of each GHBMCsi-pre model at the end of each pre-crash phase (2 seconds for abrupt brake, and 3 seconds for the turn-and-brake), was exported in terms of the nodal coordinates and used later to position the corresponding GHBMCsi model.

Position and Morphing the In-Crash Model in the Final Position of Pre-Crash Model

After performing the pre-crash simulations using GHBMCsi-pre models, a position tool (Hu et al., in press) was used to position the most appropriate GHBMCsi model in the same position. Then, the GHBMCsi model was morphed to the corresponding GHBMCsi-pre model as

explained in Section 2. A comparison of the initial posture (grey) and repositioned (yellow) posture for GHBMCsi are presented here for the brake event (Figure 17) and the brake-and-turn event (Figure 18).

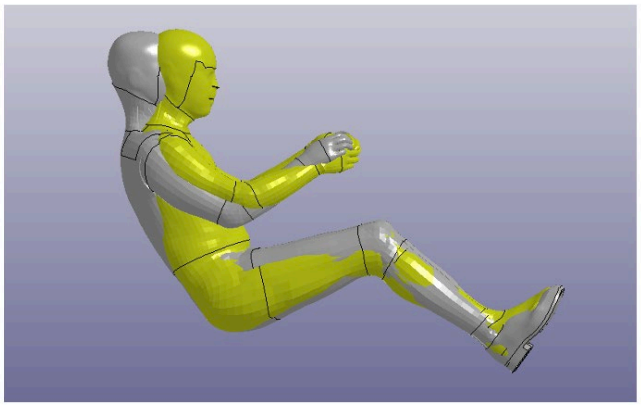

Figure 17. Comparison of initial (grey) and repositioned (yellow) posture for GHBMCsi (active level 7) for the brake event

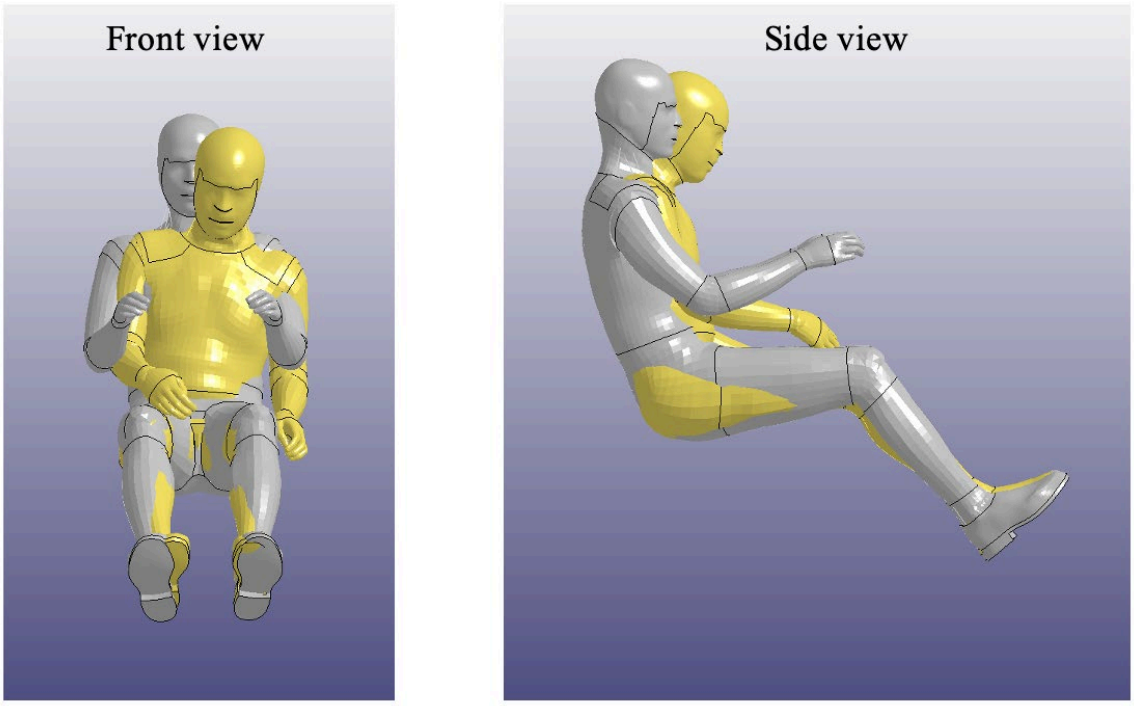

Figure 18. Comparison of initial (grey) and repositioned (yellow) posture for GHBMCsi (active level 11) for the turn-and-brake event

A Segmentation Approach to Transfer the Pre-Crash Model Kinematics to In-Crash Model

To transfer the linear velocities and angular velocities from the pre-crash model to the in-crash simulation, a switch algorithm was developed. A similar approach to that described in Öztürk et al. (2019) was used. As the pre-crash model had a reduced number of parts (e.g., the flesh parts

were missing), a direct node-to-node transfer of velocity data was not possible. Therefore, the GHBMCsi-pre models were separated into nine regions, and the corresponding center of masses (COM) were defined based on the positions extracted from GHBMCsi models (Table 7). The pre-crash simulations were re-run, and the linear/angular velocities of body regions were extracted at the end of the pre-crash simulations. Then, the data was prescribed to the corresponding regions of the GHBMCsi models as inputs at the beginning of the in-crash simulations.

Table 7. Node IDs for nine different body regions representing COMs

Body Region		**COM Node #**	**Body Region**		**COM Node #**
Head		54000001	Abdomen		54000006
Neck		54000002	Lower extremity - Left		54000007
Upper extremity - Left		54000003	Pelvis		54000008
Thorax - Axial		54000004	Lower extremity - Right		54000009
Upper extremity - Right		54000005			

The switching algorithm was tested on the GHBMCsi-pre M50 (age 20, BMI 25) model (AL7: abrupt brake maneuver, and AL11: turn-and-brake maneuver). The GHBMCsi model was positioned based on the final position of GHBMCsi-pre, and three FE simulations were performed for each pre-crash maneuver: (1) without the switch algorithm, (2) with only the initial linear velocity prescribed, and (3) with both initial linear/angular velocity prescribed. The

head, chest, and pelvis excursion were calculated based on nodal displacement of nodes attached to these body regions (Figure 19).

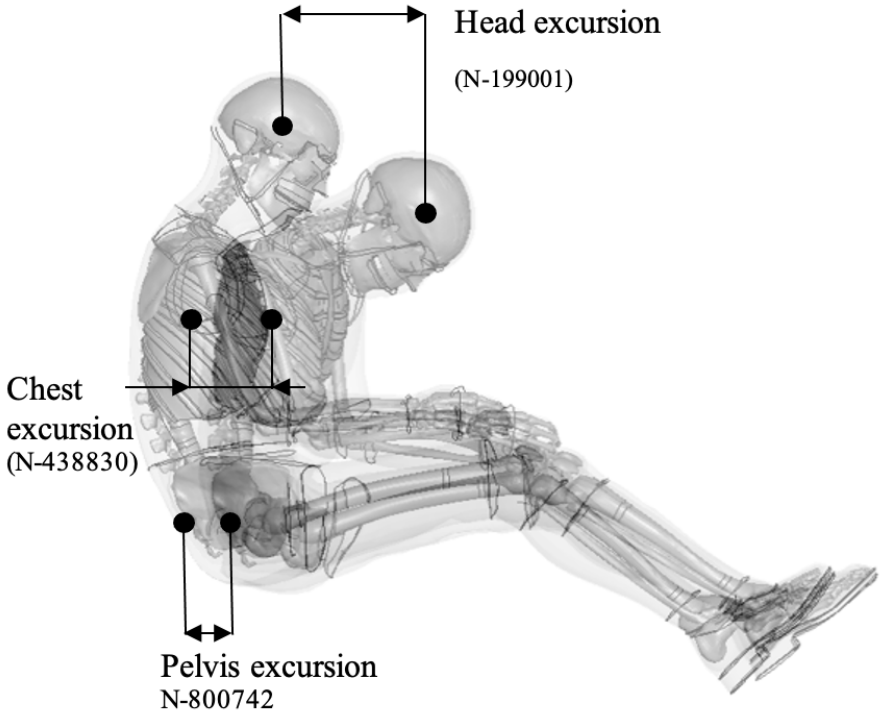

Figure 19. Calculation of M50 head, chest, and pelvis excursions during in-crash simulations

As Figure 20 shows, prescribing linear velocity data from pre-crash simulations had a relatively small effect on the head, chest, and pelvis lateral excursions (3 to 8 mm), while a slightly larger difference was observed in the longitudinal excursions (7 to 14 mm), especially in the pelvis. As expected, the effects of angular velocities were not significant considering the small values of angular velocities recorded in the pre-crash simulation for the abrupt brake event.

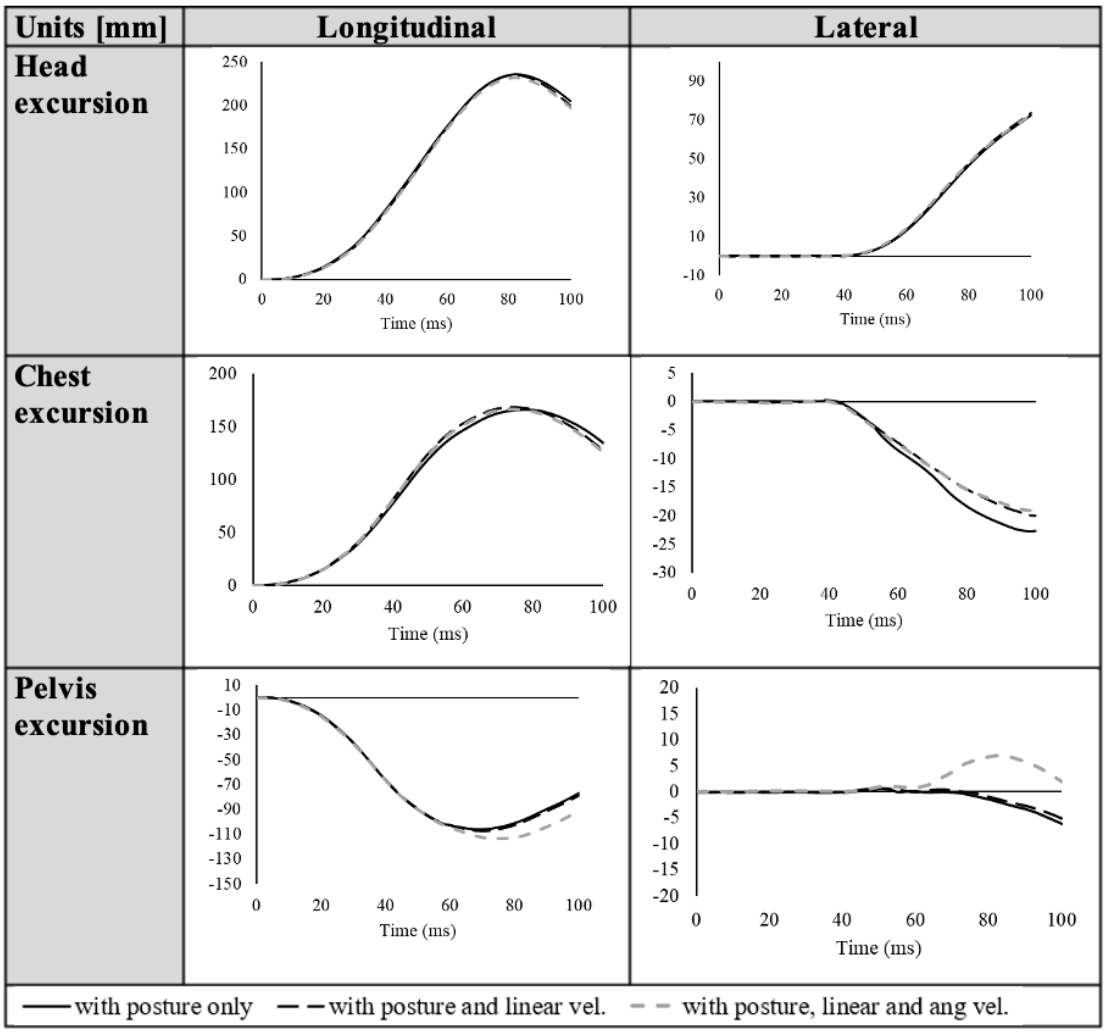

Figure 20. Male 50th percentile head, chest, and pelvis excursions in-crash simulations with a pre-crash brake event in lateral and longitudinal directions without and with prescribed pre-crash kinematics

In the simulations of the brake-and-turn event (Figure 21), differences in the longitudinal excursions between the instances "with just posture transfer" and "posture, linear, and angular velocity transfer" were greater than those in the simulations of the abrupt braking event. Due to the y-momentum, the effect of combining linear and angular velocities was stronger in the turn-and-brake events. The head and chest excursions were found to have rather high relative disparities in the longitudinal direction (68 to 75 mm). Given the higher values of angular velocities obtained in the pre-crash simulation for the abrupt turn-and-brake event, the impacts of angular velocities were, as predicted, observable in the turn-and-brake event. In the turn-and-brake event, the body-region velocities in both the x and y directions were comparable (> 10 m/s).

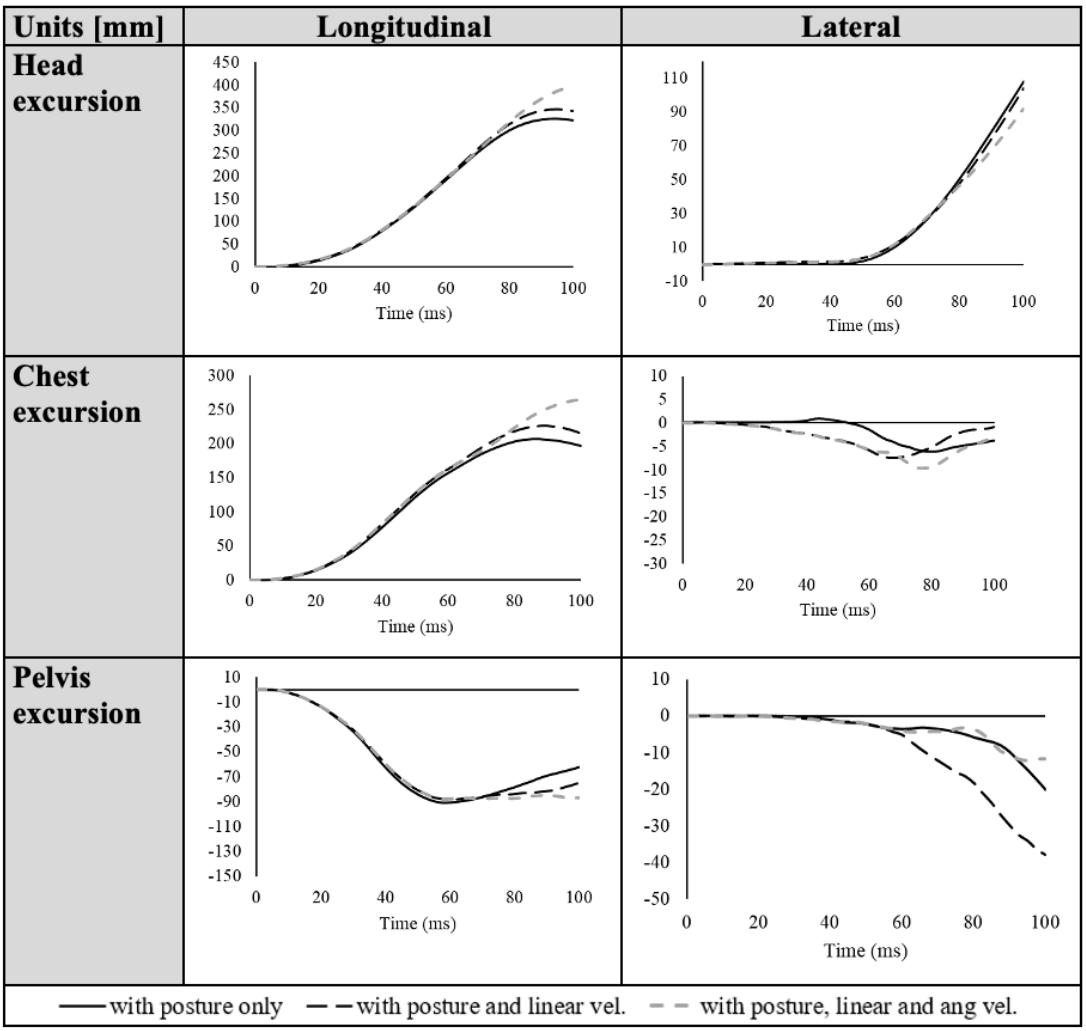

Figure 21. M50 head, chest, and pelvis excursions in-crash simulations with a pre-crash brake-and-turn event in lateral and longitudinal directions without and with prescribed pre-crash kinematics

Overall, the simulations of the GHBMCsi models with and without kinematics transfer showed some influence of the pre-crash velocity transfer on the model kinematics during in-crash simulations, especially in the turn-and-brake simulations. Therefore, in all design-of-experiments simulations, the switch algorithm was used with the transfer of both linear and angular velocities.

Passenger Air Bag Validations

A full vehicle FE model of a 2014 Honda Accord, including the vehicle interior and occupant restraint systems for the driver and front seat passenger, were developed previously (Singh et al., 2018). During that project, FE air bag models for driver and passenger occupant frontal crash protection were integrated into the full vehicle model. For validation, the vehicle model was exercised in simulation with a driver model (THOR or GHBMC) and a front passenger model (THOR) experiencing left and right oblique offset impacts against a moving barrier at a target speed of 90.12 km/h.

During this research, in preliminary simulations of the in-crash phase with an FMVSS No. 208 acceleration pulse and the simplified buck, a not physically realistic PAB behavior was observed. For example, a PAB asymmetrical deployment was observed, which may cause no contact between the 50th percentile male passenger GHBMCsi model and the passenger air bag (PAB) model (Figure 22). Therefore, the FE simulations of the left and right oblique offset impact against a moving barrier were re-run. Because similar atypical behavior was observed for the PAB model, the research team decided to revalidate the air bag model.

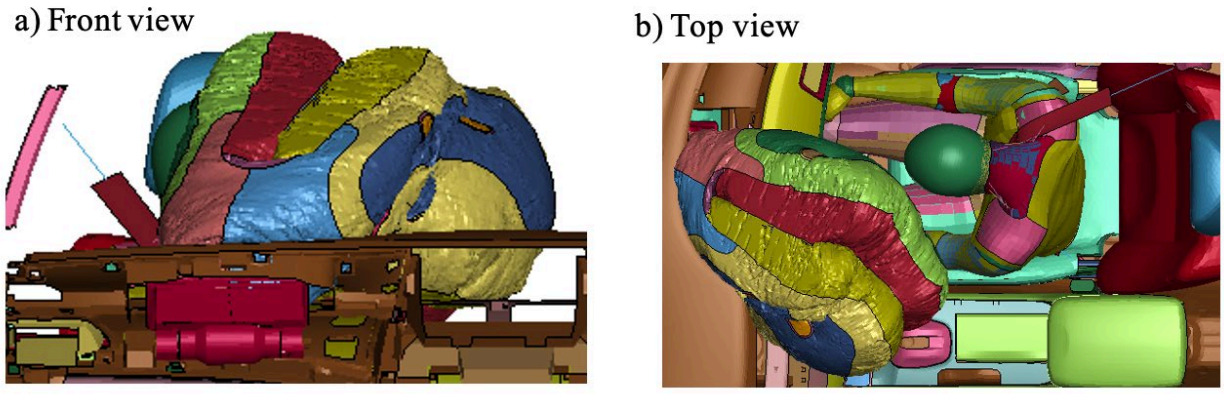

Figure 22. GHBMC – FMVSS No. 208 reduced Accord at t = 70 ms, PAB does not interact with HBM

To better understand the PAB performance in the original vehicle FE model, an impact simulation of FMVSS No. 208 was performed with the 2014 Honda Accord FE model (Figure 23), which was downloaded from NHTSA's website (NHTSA, 2022). This simulation was assigned a 35 mph (~56 km/h) initial velocity, and a rigid fixed wall. Two 50th percentile male THOR-NT dummies were seated in the driver and front passenger seats.

As is observed in Figure 24, the passenger ATD did not make any contact with the PAB during the frontal FMVSS No. 208 crash simulation, which suggested that the PAB model would require improvement. These improvements are explained in the following section.

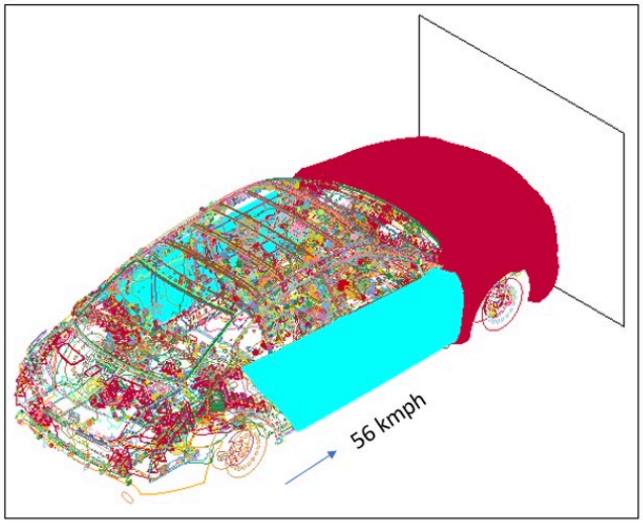

Figure 23. Simulation of FMVSS No. 208 test using 2014 Honda Accord FE model

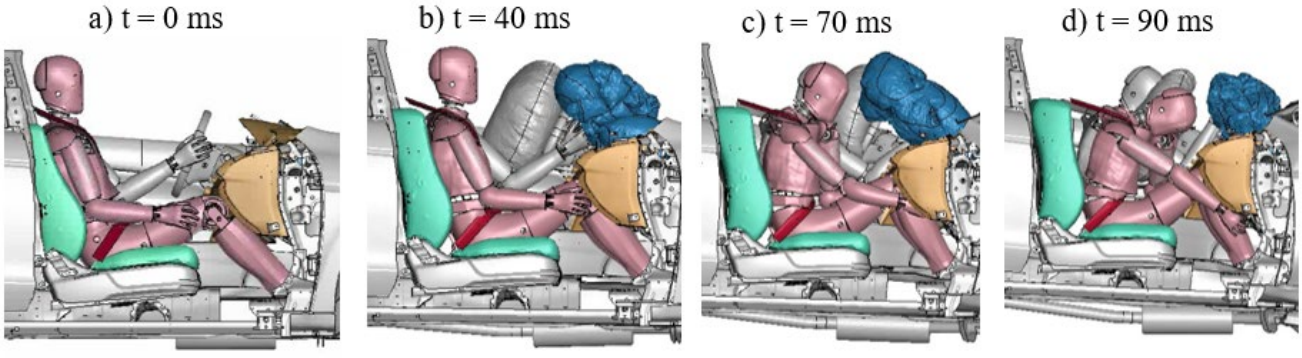

Figure 24. Frontal FMVSS No. 208 crash simulation observed no contact between the passenger ATD, THOR-M50 with PAB

Improvements of FE PAB Model in the 2014 Honda Accord

As the first improvement, the air bag control card was updated (*air bag_single_surface_contact card) by using a segment-based contact type (soft = 2) with SBOPT = 3 and DEPTH = 35, which improved the air bag contact. SBOPT = 3 led to warped segment checking, which worked better for air bag fabric contact, while DEPTH = 35 used a new method to improve penetration checking and gave a more robust shape. The original birthtime of this contact was set to 16 ms. Since we observed initial penetrations in the fabric (Fig 5-4 (a), the birthtime was set up to 0 ms as to avoid fabric penetration in the beginning of the crash and to have better deployment behavior. The contact updates described above worked much better after making these adjustments, as shown in Figure 25.

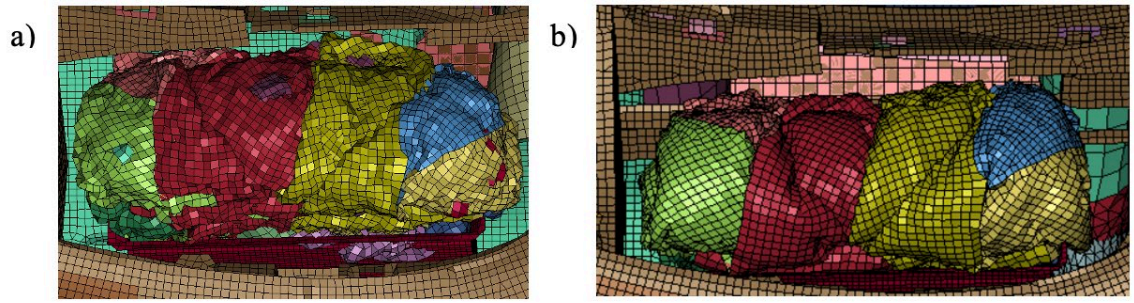

*Figure 25. Air bag at 20 ms during FMVSS No. 208 in reduced Accord car model (a) before and (b) after updating *air bag_single_surface_contact card*

Additionally, it was noted that the original car model did not include a few fabric parts, which led to surface penetration (Figure 26a). The contact set was subsequently updated, and no penetration was observed within the box and fabric (Figure 26b).

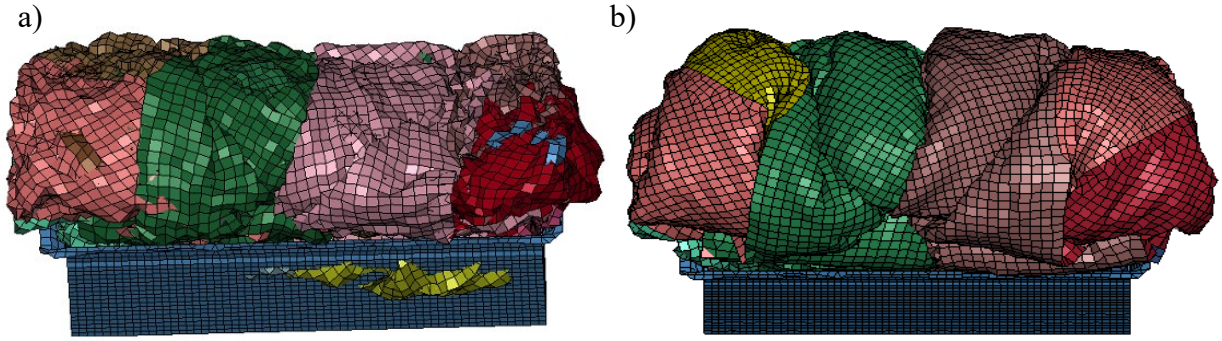

Figure 26. Air bag penetration with the box (a) initial model (b) updated model

Finally, it was observed that some PAB fabric parts were stuck in the corners during the full-crash simulation. The instrument panel was modified to avoid those corners, and PAB reference geometry was also added to the vehicle model (Figure 27).

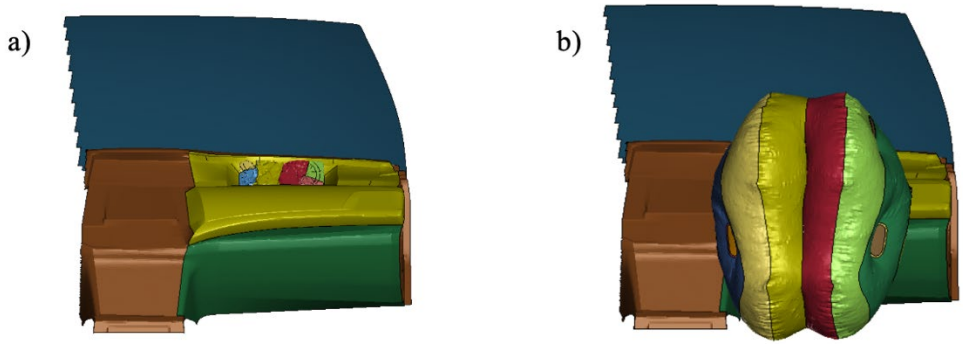

Figure 27. (a) Modified PAB and instrument panel and (b) a fully inflated PAB on the right (t = 70 ms)

Finally, the latest version of PAB showed a symmetric deployment and improved contact with the 5th female HIII model (front passenger) during full frontal impact (Figure 28). It should be noted that the research team received support from ZF researchers in the last phase of air bag improvements.

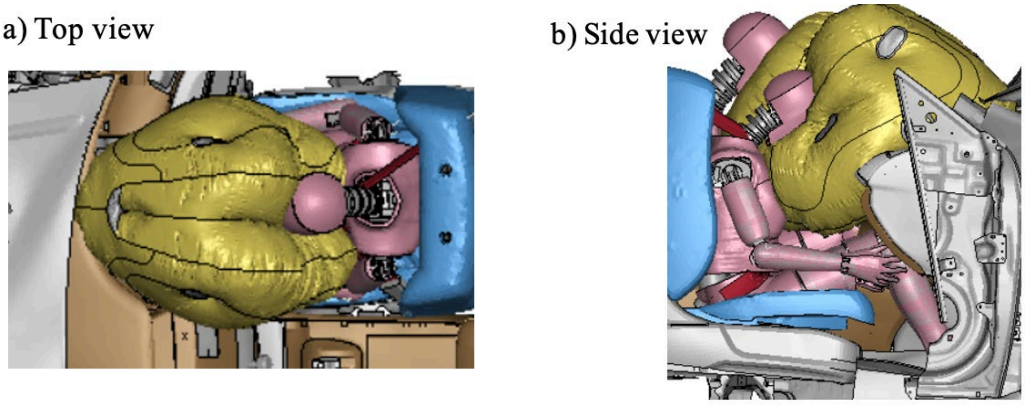

Figure 28. Frontal Impact with modified PAB at t = 80 ms in the full vehicle model with HIII M50 on driver and passenger side

Drop-Tower Test Validations

The performance of the updated PAB was evaluated in a drop-tower test setup (Figure 29). In the validation procedure, the folded PAB was fitted in the PAB housing sub-system and the PAB was inflated to replicate the drop tower test data. An impactor of mass 36.3 kg was released from a certain height with an initial velocity of 4.7 m/s, reaching a speed of 5.4 m/s at the time of impact.

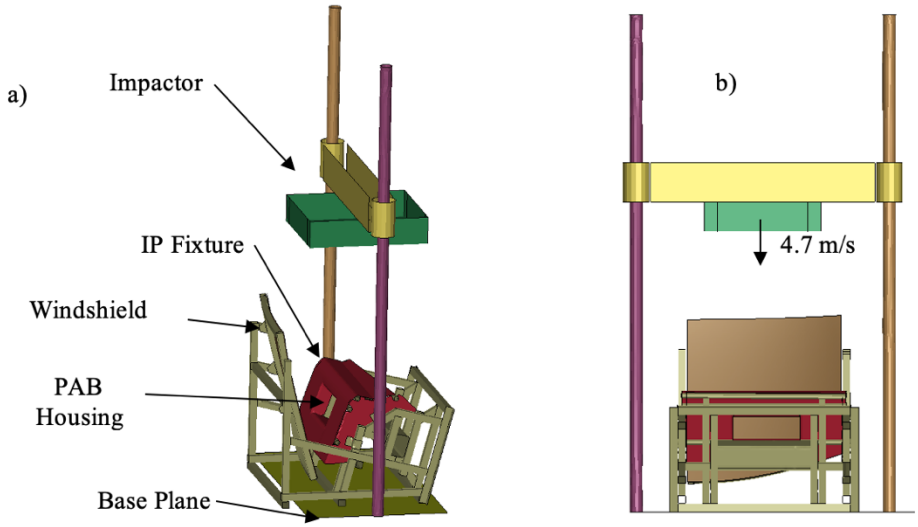

Figure 29. (a) Isometric view of the drop-tower test setup for the PAB and (b) Front view of the setup with the impactor dropped from a certain height with an initial downward speed of 4.7 m/s

As seen in Figure 30, the updated PAB kept its air well and showed a good correlation with test data in terms of impact force at up to 350 mm of vertical displacement (Figure 31).

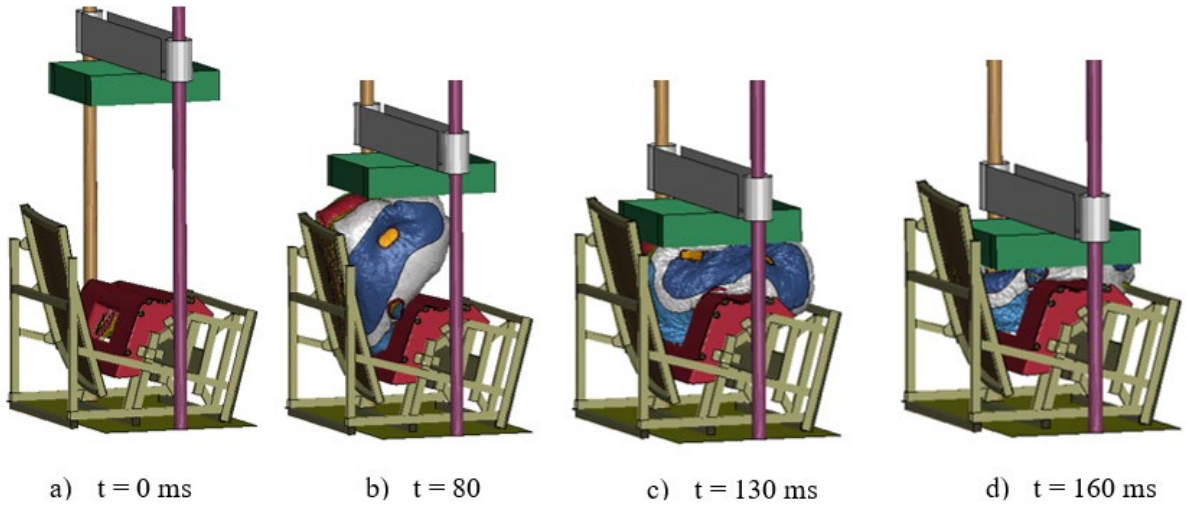

Figure 30. PAB deployment at different timesteps during the drop tower test simulation

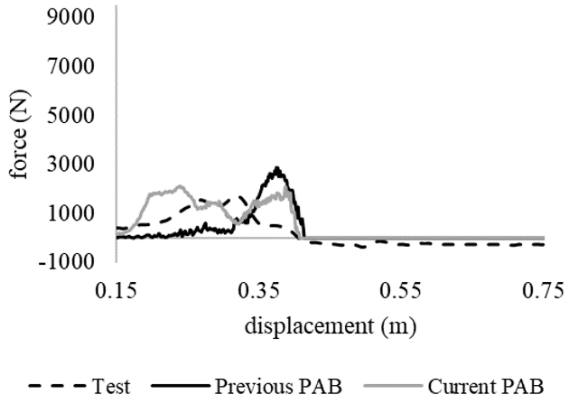

Figure 31. Force-displacement curve for the current PAB simulation compared with drop tower test data

The previous PAB and the current results with the updated PAB were compared to test data in terms of vertical displacement, velocity, and acceleration. As the results indicate, the current PAB performed better than the previous PAB model. While the acceleration curve of the previous PAB fell flat, the current PAB maintains a robust shape.

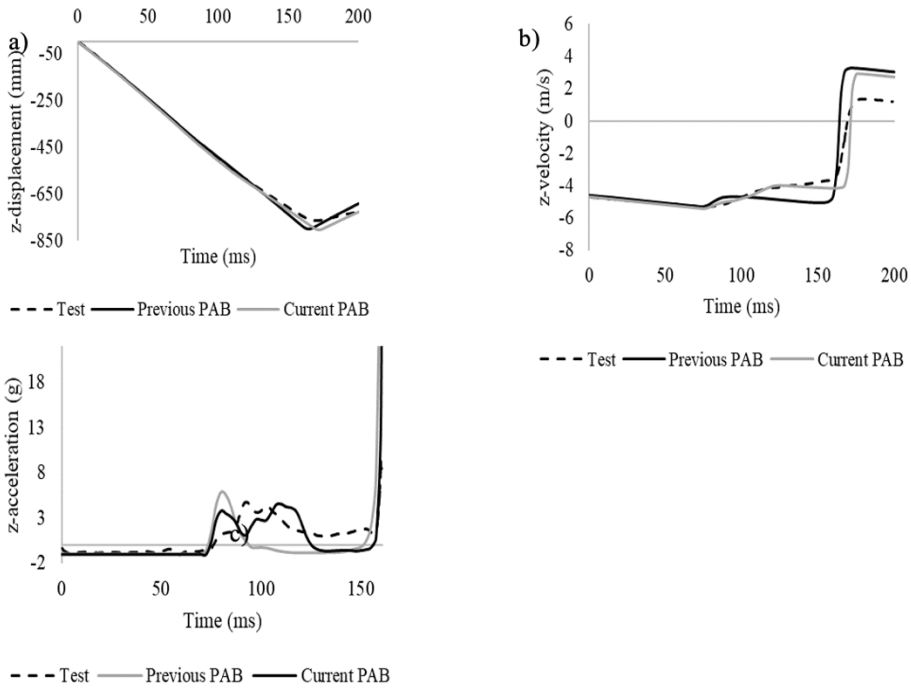

Figure 32. Drop tower test impactor's (a) displacement, (b) velocity, and (c) acceleration compared with the previous and the current (corrected) passenger air bag simulations

Frontal Impact Simulations

The FE frontal impact simulation using a 2014 Honda Accord FE model with updated PAB model (Figure 23) was re-run (FMVSS No. 208 test). As in testing, a male 50th percentile H-III was seated in the driver's seat and female 5th percentile H-III in the front passenger seat (Figure 33).

Figure 33. Honda Accord vehicle model with H-III M50 in the driver seat and H-III F05 in the passenger seat

As seen from the top and right side view of the crash at t = 80 ms, the head of the H-III ATD on the passenger side rested almost symmetrically with the PAB (Figure 34). The shape and size of the PAB also looked symmetric and robust.

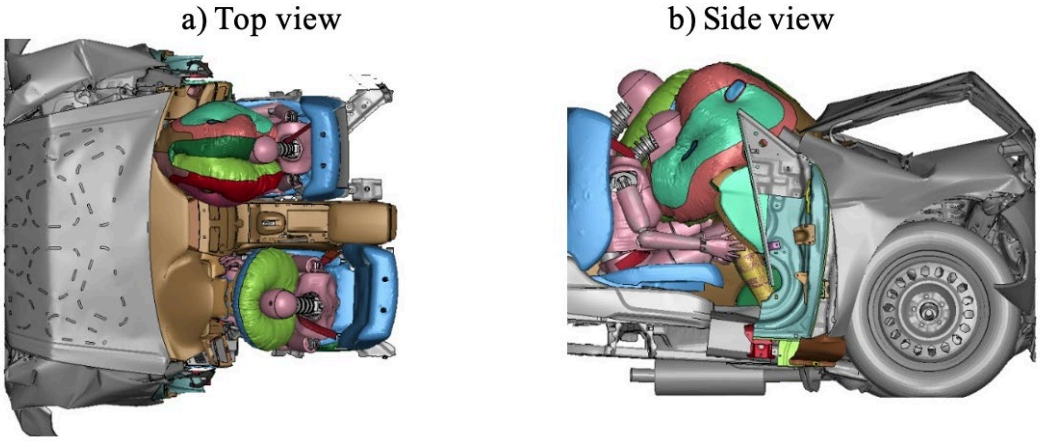

Figure 34. Top view and right view during full frontal crash (56 kmph) with a H-III M50 in the driver seat and H-III F05 in the passenger seat

As the update of the PAB model had an insignificant influence on the driver-vehicle interaction, only the results corresponding to passenger-vehicle interaction are presented in this section. However, the driver data can be found in Appendix A.

Because of the proximity of the passenger ATD to the dashboard, the first contact was made with the air bag at around 50 ms when the PAB hit the ATD's face, causing a sharp dip in the head x-acceleration. After the first contact, the PAB slipped off the passenger's face and the ATD's head kept accelerating forward. Around 80 ms, the PAB was fully inflated, and the ATD head rested on the PAB, leading to deceleration of the passenger's head. The PAB in this test deployed symmetrically and kept its air within, as seen during the real crash (Chiu, 2012). The head struck the PAB in the center (Figure 35a). In simulations with the previous PAB, the deployment was not symmetric and robust, and the PAB lost air very quickly; hence there was no tangible impact with the PAB (Figure 35b).

	Top view	Side view
Previous PAB model	a) 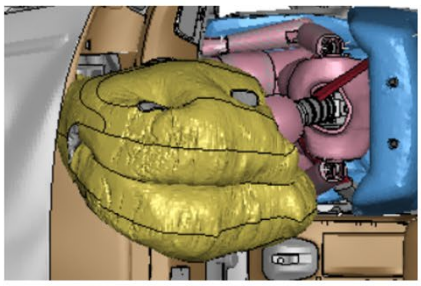	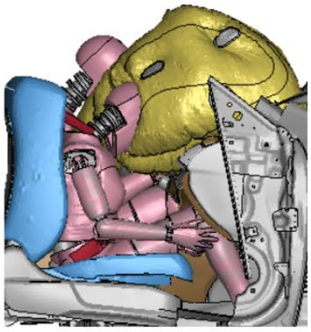
Current PAB model	b) 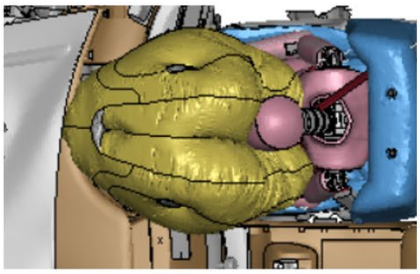	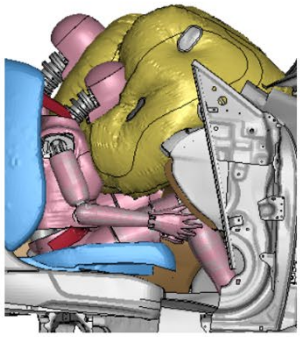

Figure 35. FE simulation with (a) previous PAB model (b) modified PAB model at t = 80 ms in a full vehicle simulation with H-III 5th female on the passenger side

Frontal Impact With Updated PAB – Passenger Correlation Results: H-III F05 Simulation

The head, chest, and pelvis accelerations obtained from FE simulations with the updated PAB model were compared to corresponding data recorded in the FE simulation with the previous PAB model and test data, respectively (Figure 36, Figure 37, Figure 38). The better interaction between the ATD head and updated PAB model was reflected in the head's center of gravity (CG) response. For example, the head acceleration time histories recorded with the updated PAB model showed better correlation (especially in x/y directions) with test data than the corresponding data recorded in the FE simulation with the previous PAB model.

The responses of the pelvis and chest in the simulation with the updated PAB model were very much like the corresponding data from the impact simulation with the previous PAB model, which consequently was reflected in their close CORA scores (Table 8).

The occupant correlation results for the frontal impact with the modified PAB H-III M50 simulation are presented in Appendix A.

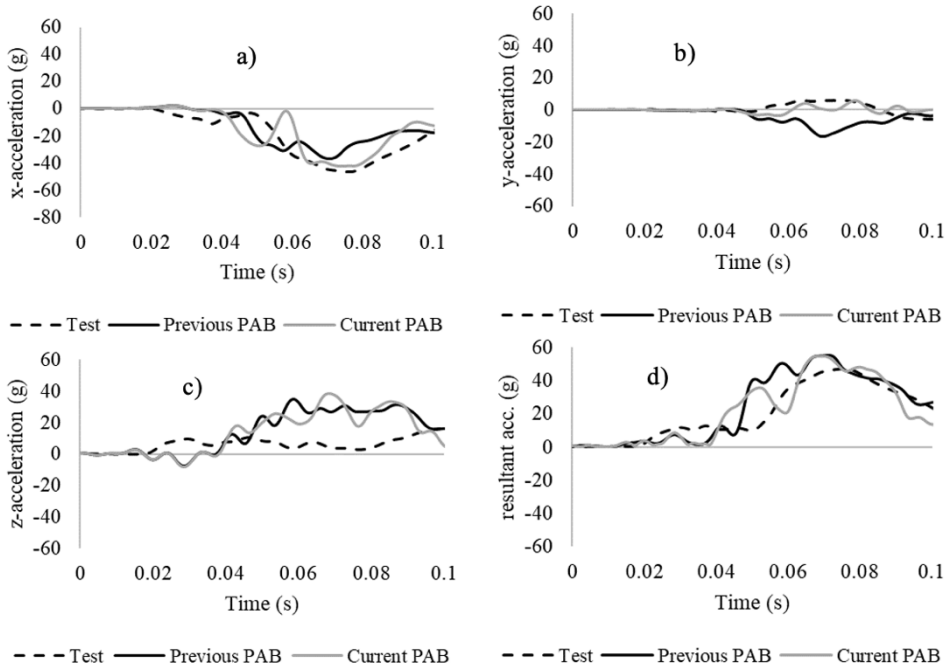

Figure 36. Comparison of passenger's head CG (a) x-acceleration, (b) y-acceleration, (c) z-acceleration, and (d) resultant acceleration

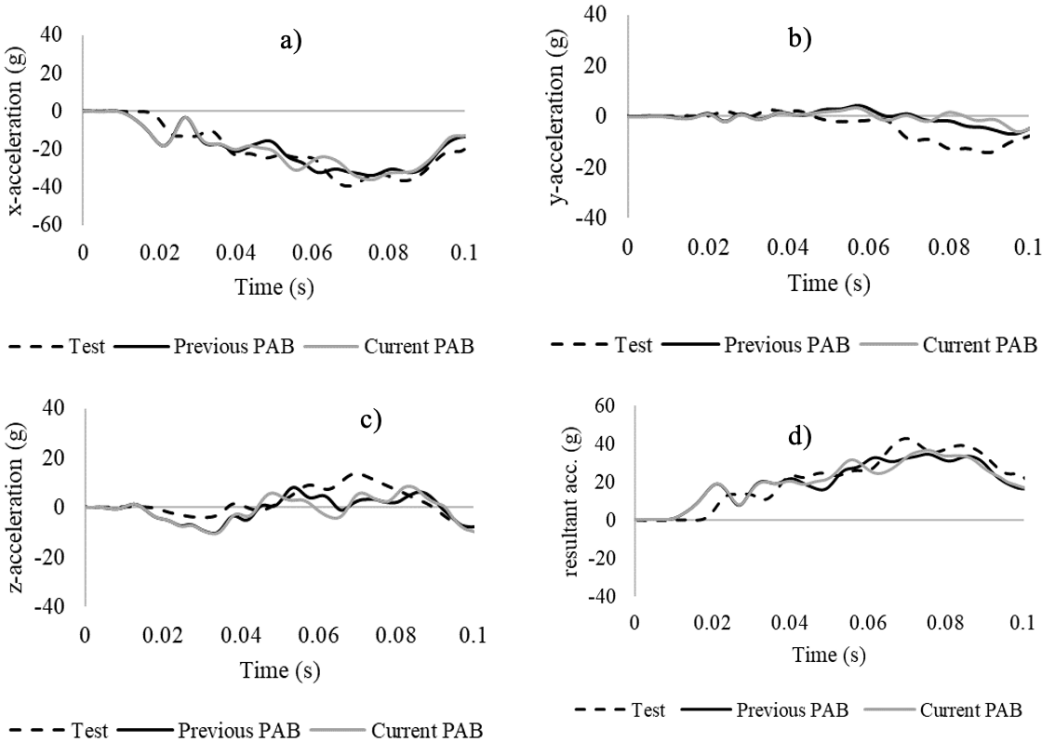

Figure 37. Comparison of passenger's chest CG (a) x-acceleration, (b) y-acceleration, (c) z-acceleration, and (d) resultant acceleration

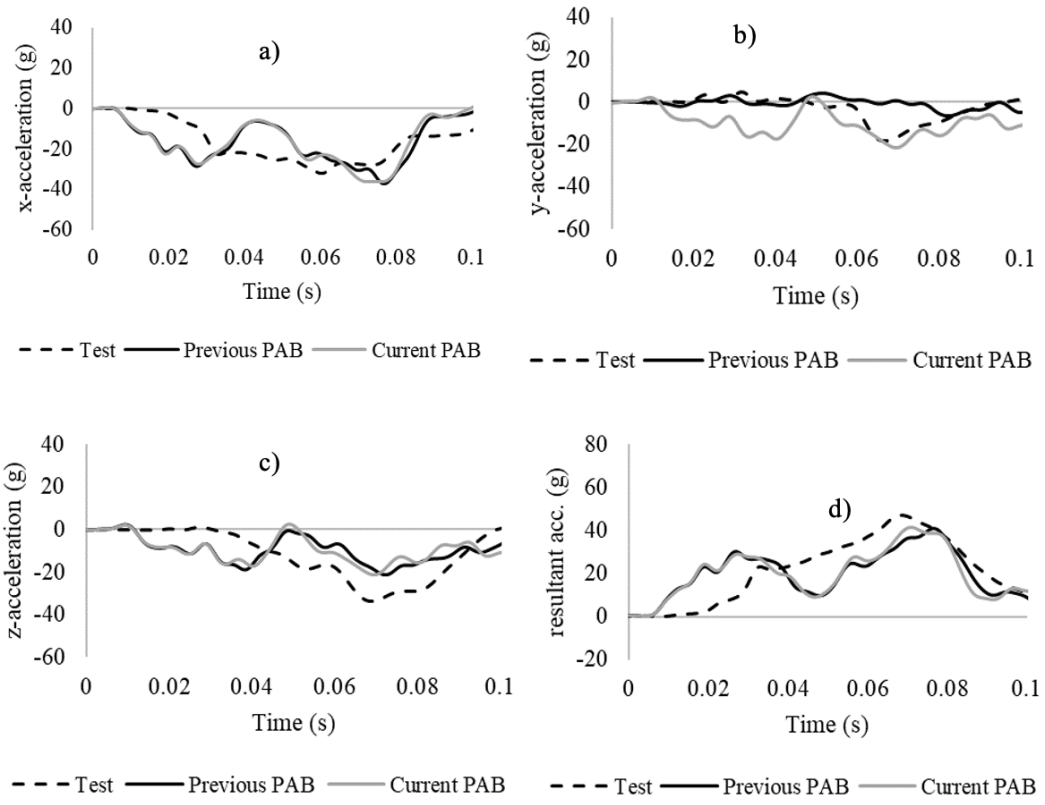

Figure 38. Comparison of passenger's pelvis CG (a) x-acceleration, (b) y-acceleration, (c) z-acceleration, and (d) resultant acceleration

Table 8. CORA score comparison: Previous air bag (left) with current air bag (right)

Curve (Passenger)	Previous Air Bag	Current Air Bag
Head CG X-Acceleration	0.80	0.82
Head CG Y-Acceleration	0.30	0.44
Head CG Z-Acceleration	0.40	0.36
Chest CG X-Acceleration	0.95	0.96
Chest CG Y-Acceleration	0.55	0.54
Chest CG Z-Acceleration	0.67	0.63
Pelvis CG X-Acceleration	0.72	0.72
Pelvis CG Y-Acceleration	0.60	0.61
Pelvis CG Z-Acceleration	0.67	0.65

Head Rotational Velocity Comparison

Rotational velocity plays a key role in injury calculations, especially in BrIC. The passenger head angular velocity resultant and z-direction component were compared along with the resultant rotation of the head. A comparison of the results shows that the modified PAB reduced the ATD's angular velocity upon interacting with the air bag. As seen in the z-direction comparison of angular velocity (Figure 0-18a), the ATD's head rests on the air bag, thus

bringing the rotational velocity to zero. In the resultant rotation comparison (Figure 39c), the head rotation was reduced after 80 ms when the head came to rest on the air bag.

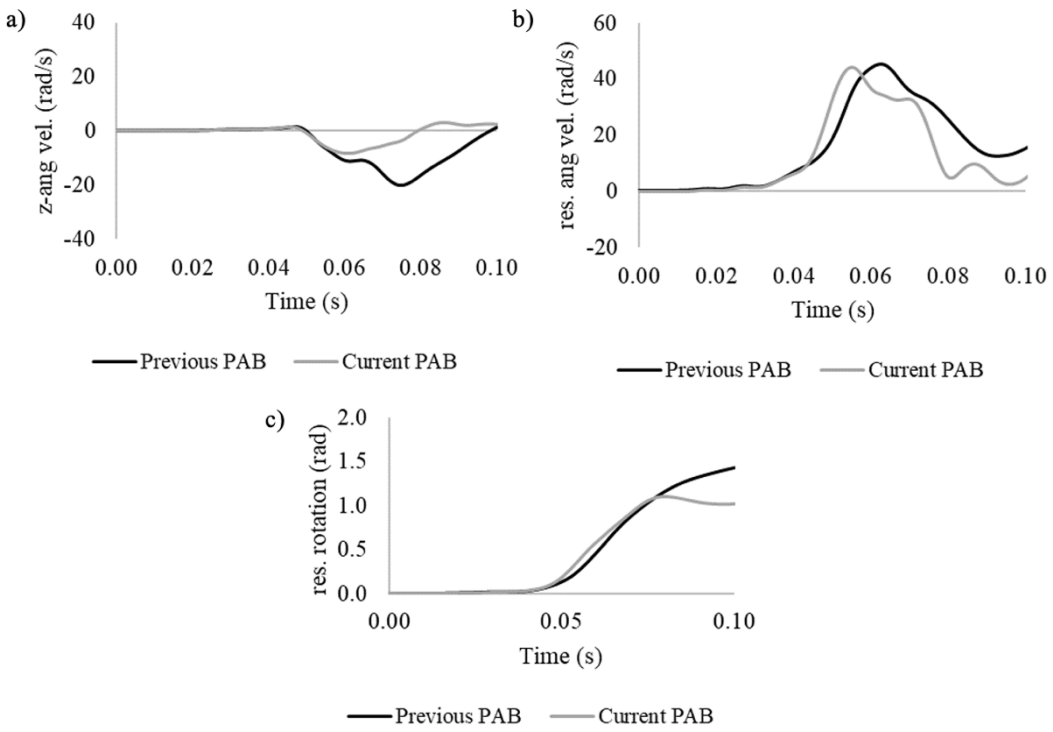

Figure 39. Passenger head CG (a) angular velocity in Z-direction, (b) resultant angular velocity, and (c) resultant head rotation compared from previous and current PAB

Oblique Impact Simulations

The behavior of the updated PAB model in terms of interaction with the front passeger was evaluated against test data recorded in an oblique offset left impact test. This test was designed to verify the vehicle's crashworthiness in offset frontal impact crash instances in order to safeguard occupants. In this test, the stationary 2014 Honda Accord FE model was struck by a 2,490.2 kg oblique moving deformable barrier traveling at a target speed of 90.12 km/h. Prior to testing, the struck vehicle was positioned 15 degrees relative to the moving barrier and struck 35 percent of the left of the vehicle (Figure 40). Two male 50th percentile THOR-NT dummies were seated on both the driver and passenger sides for the oblique test (Figure 41).

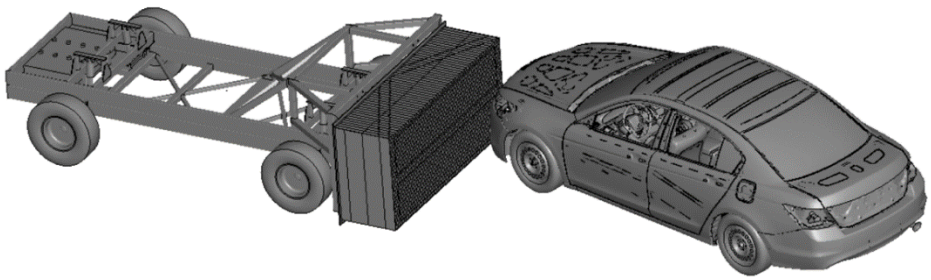

Figure 40. NHTSA oblique test left setup

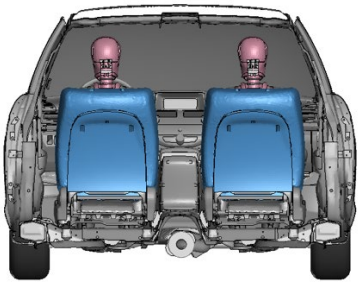

Figure 41. Male 50th percentile THOR-NT on both the driver and passenger side seated in the full vehicle model

As the update of the PAB model had insignificant influence on the driver-vehicle interaction, only the results corresponding to the passenger-vehicle intercation are presented in this section. However, the driver data can be found in Appendix A.

Oblique Impact Left With Updated PAB – Passenger Correlation Results: THOR M50 Data

The passenger's head and pelvis acceleration of the THOR M50 ATD during a left oblique crash simulation with the updated PAB was compared with corresponding data from the original PAB model. Comparison results showed that the current PAB simulation did not significantly improve the correlation of head/pelvis acceleration with test data in the oblique scenario as compared to the previous PAB results (Figure 42, Figure 43). The improved performance from the current PAB was expected in the full-frontal case, which was the setup used in this project's design-of-experiment.

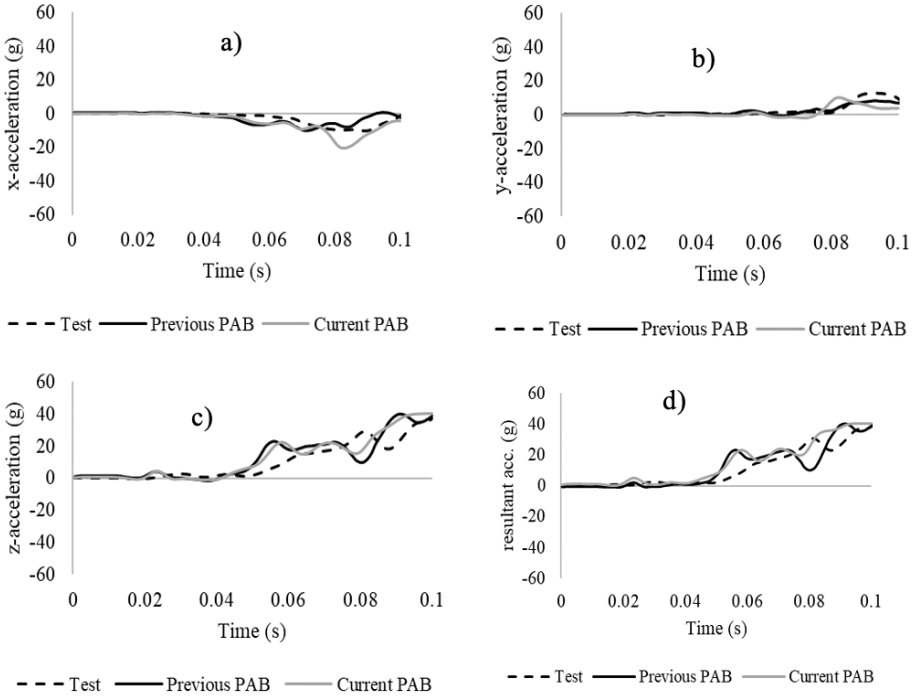

Figure 42. Passenger's head CG (a) x-acceleration, (b) y-acceleration, (c) z-acceleration, and (d) resultant acceleration

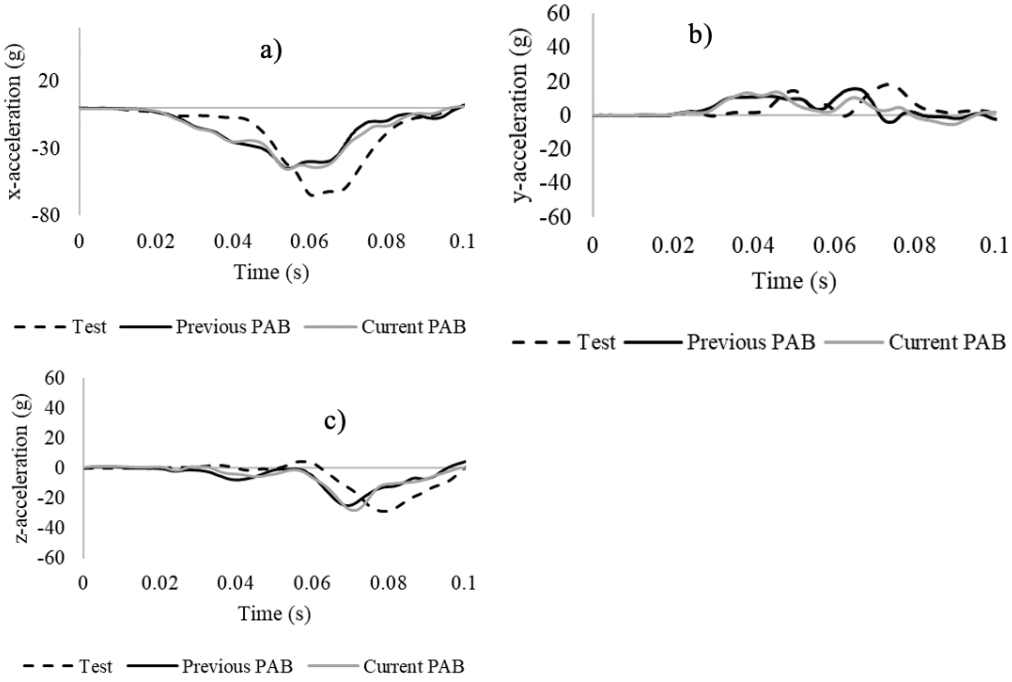

Figure 43. Passenger's pelvis CG (a) x-acceleration, (b) y-acceleration, and (c) z-acceleration

The passenger ATD's upper belt forces and femur forces recorded in the FE simulation with the updated air bag model were compared with the test data and FE data from the previous PAB model (Figure 0-23). Again, the FE data from the current PAB were akin to the corresponding data from the previous PAB model.

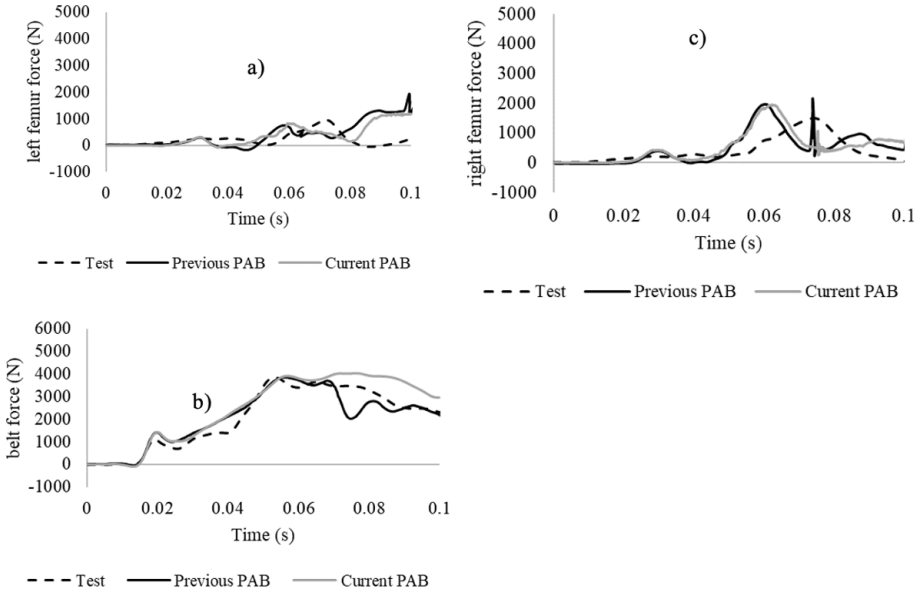

Figure 44. Comparison of front passenger's (a) femur left force, (b) femur right force, and (c) upper belt force (test data, FE data with previous PAB, and current PAB)

The driver correlation results for the oblique impact left from the modified PAB THOR M50 simulation are presented in Appendix A.

Oblique Impact Right With Updated PAB – Passenger Correlation Results: THOR 50M Data

There was a slight improvement in head x-acceleration using the current PAB. The comparisons of head y- and z-accelerations from the current and previous PAB with the test data were quite similar (Figure 45).

There was a slight improvement in pelvis y-acceleration using the current PAB. The comparison of the pelvis x- and z-accelerations from current and previous PAB with test data were also quite similar (Figure 46).

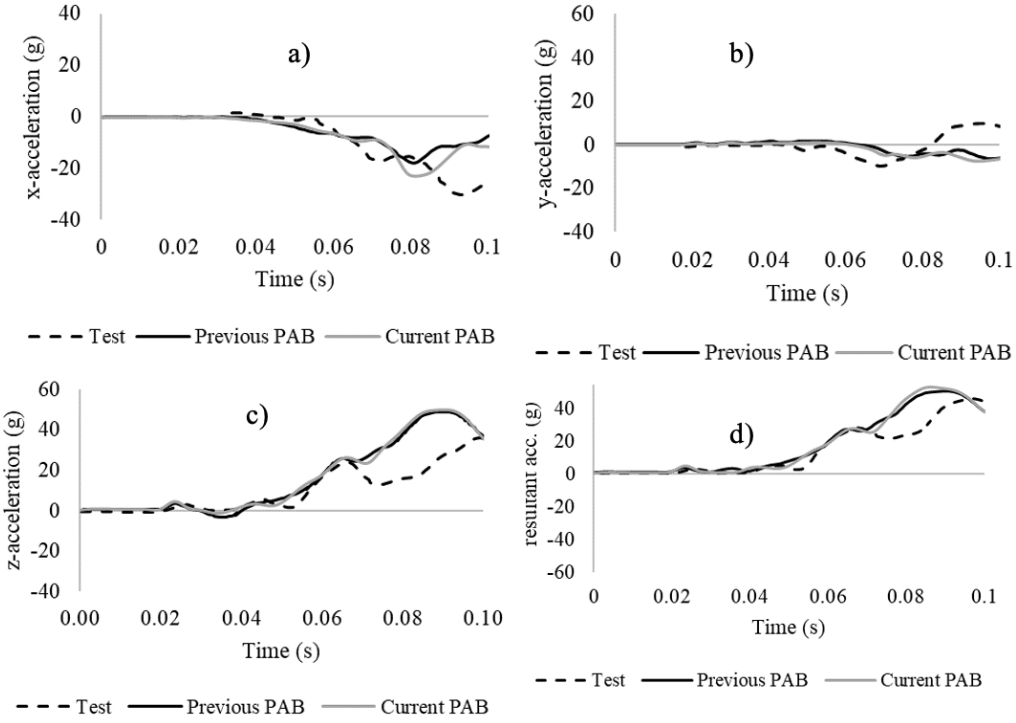

Figure 45. Comparison of passenger's head CG (a) x-acceleration, (b) y-acceleration, (c) z-acceleration, and (d) resultant acceleration in right oblique impact

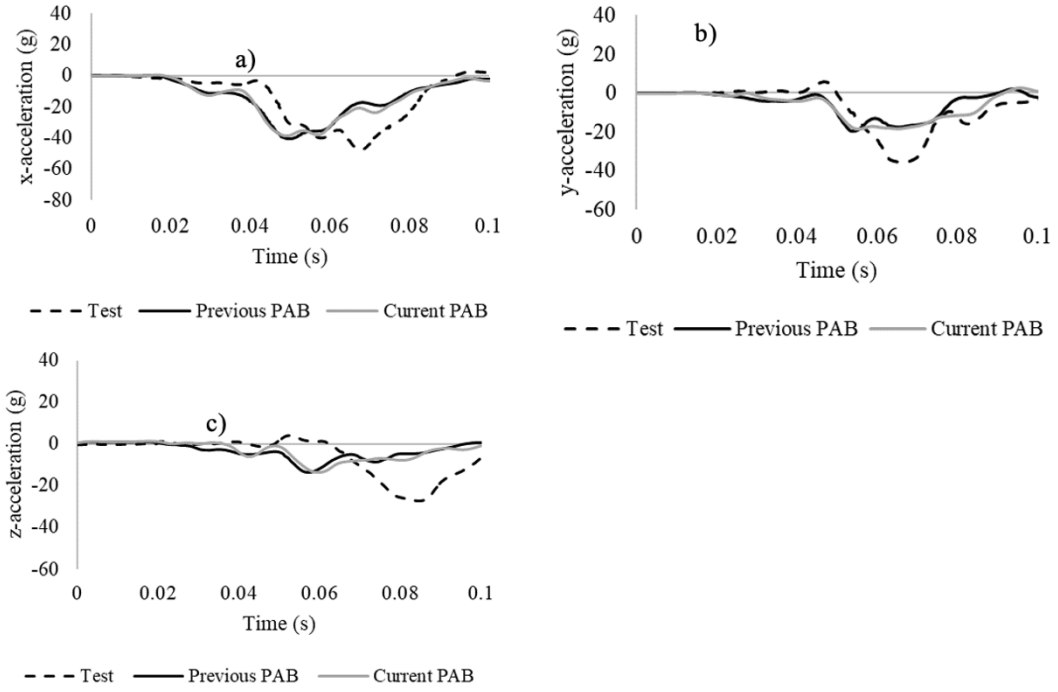

Figure 46. Comparison of passenger's pelvis CG (a) x-acceleration, (b) y-acceleration, and (c) z-acceleration in right oblique impact

Figure 47 shows that the current PAB performed better regarding the left femur force in comparison with the test data as compared to the previous PAB's performance. Few differences were observed in the comparison of belt forces and right femur forces.

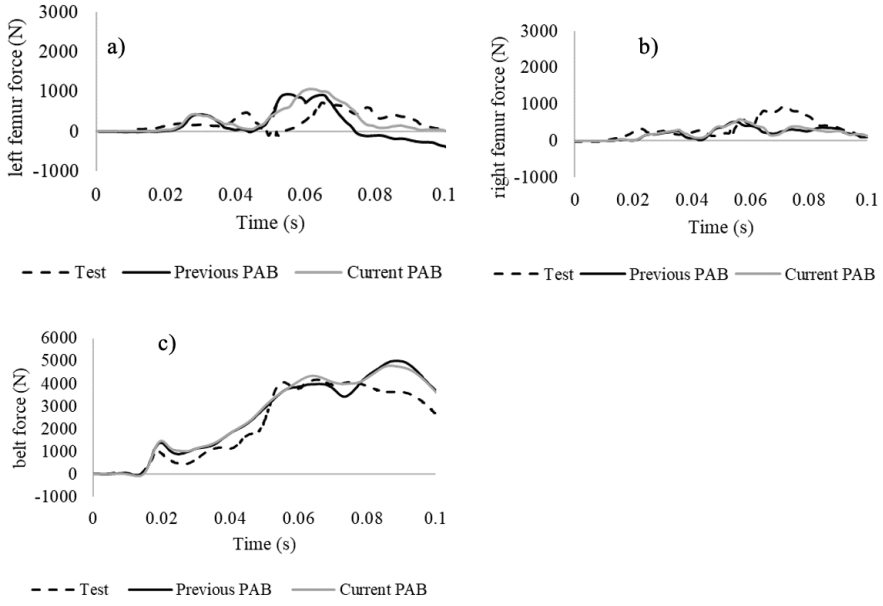

Figure 47. Comparison of passenger's (a) upper belt force, (b) femur left force, and (c) femur right force with results from test, previous PAB, and current PAB in right oblique impact

The driver correlation results for the oblique impact right with modified PAB THOR M50 simulation are presented in Appendix A.

Design of Experiments

To investigate how variations in passenger's anthropometry, along with seat positioning and two (2) common pre-crash maneuvers, influence passengers' risk of injury during a typical frontal crash, a design-of-experiment study was developed. The design-of-experiment variables (Figure 48) were selected based on the data/models available from previous research (e.g., occupant morphed models) (Hu et al., in press, 2019) and literature data (Rawska et al., 2020).

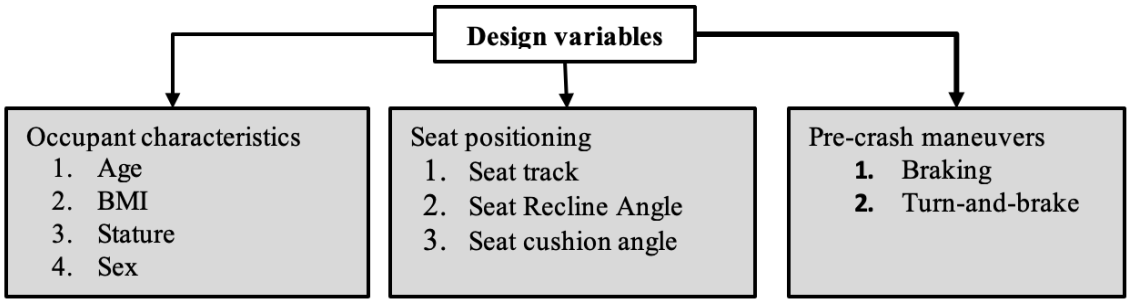

Figure 48. Design variable used in design-of-experiments study

As previously mentioned (see Section 2), a set of 12 HBMs (Hu et al., in press) was used in previous research to represent variations in front passengers. The ages considered were a 20- and 70-year-old, and the BMIs examined were 25 (normal) and 40 (obese). The GHBMC simplified models corresponding to a 5th percentile female, 50th percentile male, and 95th percentile male were considered as baseline models.

The passenger posture was varied by seat characteristics (Figure 49) in terms of seat cushion angle, seat back angle, and seat track position. For the seat cushion angle, level 0 was chosen as the default/lowest angle for the passenger seat. Level 1 added 10° to the standard seat cushion angle. Similarly, for the seat back angle, level 0 was chosen as the default/lowest angle for the passenger seat (measured with a vertical axis). Level 1 added 20° to the standard seat back angle.

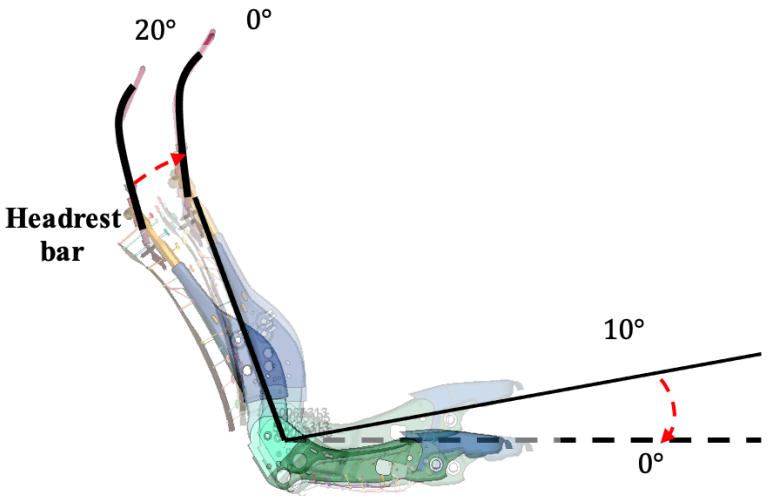

Figure 49. Right view on passenger side showing seat back angle and seat cushion angles considered in the design-of-experiment scheme

For the seat track position, level 0 was chosen as a position where the distance between the knee and dashboard was around 10 mm. Level 1 was defined as the farthest point from the dashboard (around 130 mm), determined based on the male 95th GHBMCsi. The total fore-aft range of seat track position is displayed in Figure 50.

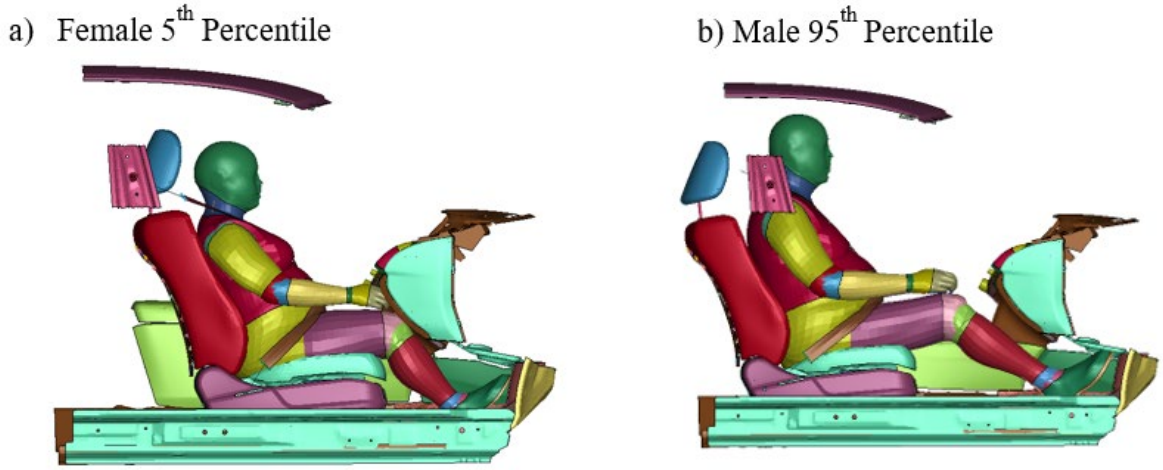

Figure 50. Right view on passenger side showing seat track position: (a) Level 0 (~10 mm); i.e., closest to dashboard, and (b) level 1 (~130 mm); i.e., farthest from dashboard

Finally, two pre-crash maneuvers were considered—brake and turn-and-break—based on the data available from previous research. All levels of seat and maneuver type variables are provided in Table 9.

Table 9. Definition of seat characteristic levels, maneuver type, and sexes used in the design-of-experiment

Levels	**0**	**1**
Seat track position	~ 10 mm	~ 130 mm
Seat Recline Angle	0°	20°
Seat Cushion Angle	0°	10°
Maneuver type	Brake	Turn-and-brake

The number of simulations for a full factorial scheme is: 12 x 2 x 2 x 2 x 2 = 196 simulations. To reduce the computational effort, a reduced factorial scheme, Latin hypercube sampling, was used, as recommended in Montgomery (2019), so the total number of simulations was 55 (See Table 10).

Table 10. A reduced factorial design-of-experiments scheme (Latin hypercube sampling-55 simulations full factorial –192 simulations)

Point	Occupant Characteristics				Seat Characteristics			Manuever level
	Age	Gender	Height	BMI	Seat track level	Seat Recline Angle level	Seat Cushion Angle level	
1	20	1	152	25	1	0	1	0
2	70	1	152	40	1	0	1	0
3	20	0	189	40	1	0	1	0
4	20	1	152	25	1	1	1	1
5	70	0	176	40	1	1	1	0
6	20	0	176	25	1	0	1	0
7	70	1	152	25	0	1	0	1
8	20	0	176	40	1	1	1	0
9	70	0	189	25	0	1	1	0
10	20	0	189	40	1	1	1	1
11	20	1	152	40	0	0	0	0
12	20	1	152	40	0	1	0	1
13	70	0	176	25	1	1	0	0
14	20	0	189	40	0	0	1	1
15	70	0	176	25	1	1	0	1
16	20	0	189	25	1	1	0	0
17	20	0	176	40	0	0	0	0
18	70	0	176	25	0	1	1	0
19	20	0	189	25	0	0	1	0
20	20	1	152	40	1	1	0	1
21	70	0	189	40	1	0	1	1
22	20	0	176	25	1	1	0	0
23	20	0	176	40	0	1	0	0
24	20	0	176	40	1	0	1	1
25	70	0	176	40	0	0	0	1
26	20	0	176	25	0	1	1	0
27	20	0	176	40	0	0	1	1
28	70	0	189	25	0	0	1	0
29	20	0	189	40	1	1	0	1
30	70	0	176	40	0	1	0	1
31	70	1	152	25	1	0	1	1
32	20	0	176	25	0	0	0	1
33	20	1	152	40	0	0	0	1
34	70	0	176	40	1	1	1	1
35	20	1	152	25	0	0	0	0
36	20	0	176	40	1	1	0	0
37	70	0	189	40	1	1	1	0
38	70	0	176	25	0	0	0	0
39	70	1	152	25	0	0	1	1
40	70	0	189	25	1	0	0	0
41	70	1	152	40	1	1	0	1
42	70	0	176	40	0	1	0	0
43	70	0	176	25	1	0	1	1
44	20	0	189	25	1	1	0	1
45	70	1	152	40	1	0	1	1
46	70	1	152	40	0	1	1	1
47	20	0	189	25	1	1	1	0
48	20	0	189	40	1	0	0	1
49	70	0	189	25	0	0	1	1
50	70	0	189	25	0	1	0	1
51	20	1	152	40	0	1	1	0
52	70	1	152	40	1	0	0	1
53	70	1	152	25	0	0	0	1
54	70	1	152	25	1	0	0	1
55	70	1	152	25	0	0	1	0

During the in-crash phase, a full-frontal crash of 35 mph (35 mph (~56 km/h)) was simulated, with the acceleration pulse corresponding to a 2014 Honda Accord during FMVSS No. 208 crash testing (Figure 51).

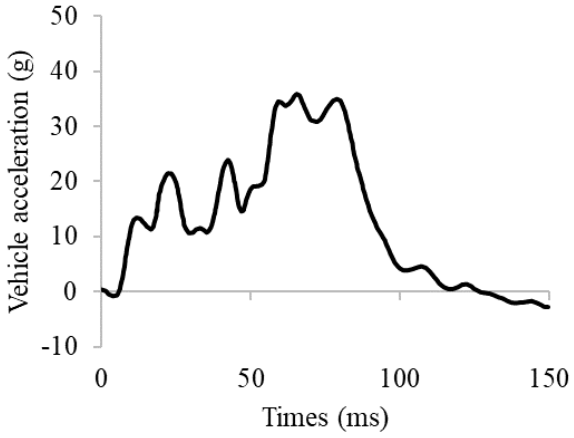

Figure 51. Acceleration curve for a full-frontal crash of a 2014 Honda Accord at 35 mph (35 mph (~56 km/h)) per FMVSS No. 208 guidelines

The GHBMCsi (simplified) model was used, which shows relatively good injury predictions relative to the GHBMC-O (detailed) model (Schwartz et al., 2015).

Injury Risk Assessment and Analysis

In this section, the injury metrics recorded in all design-of-experiment simulations—such as HIC15, BrIC, Nij, chest compression, abdomen viscous criterion (VC), and femur force—were used to calculate the passenger's risk of serious injuries (AIS 3+). Then, FE simulations were included into several sets to better understand the injury risks for certain passenger anthropometry relative to including or not of the pre-crash phase in the simulation.

Male 50th Percentile (age 20, BMI 25)

For example, the three FE simulations (without pre-crash, with pre-crash brake, and with pre-crash brake-and-turn) corresponding to a frontal collision with the 50th percentile male simplified model seated in the nominal position (cushion/back seat angles = 0) and the track position close to the dashboard were analyzed. The model responses, especially in terms of head CG kinematics, were compared to better understand the influence of including a pre-crash phase.

As seen in the M50 (age: 20, BMI: 25), simulation of a frontal crash without the pre-crash phase (Figure 52a), the passenger is in a standard position at the beginning of the simulation, and then contacts the PAB at about 70 ms. On the other hand, in the simulations that included the pre-crash maneuvers, the initial posture of the passenger already had a forward displacement (higher in the brake case [Figure 52b] than in the turn-and-brake case). The resultant head acceleration in the brake case had a sharp peak at around 45 ms because of the contact of the GHBMC with the air bag, whereas for the turn-and-brake case, the rise/initial contact was around 48 ms. Initial contact was followed by a drop in the acceleration because of the transfer of kinematic energy from the head to the air bag. In the FE simulation without pre-crash maneuvers and corresponding pre-crash simulation, the head contacted the PAB later (70 ms), leading to a later head acceleration with its peak almost 30–33% higher than in simulations with the pre-crash (Figure 53).

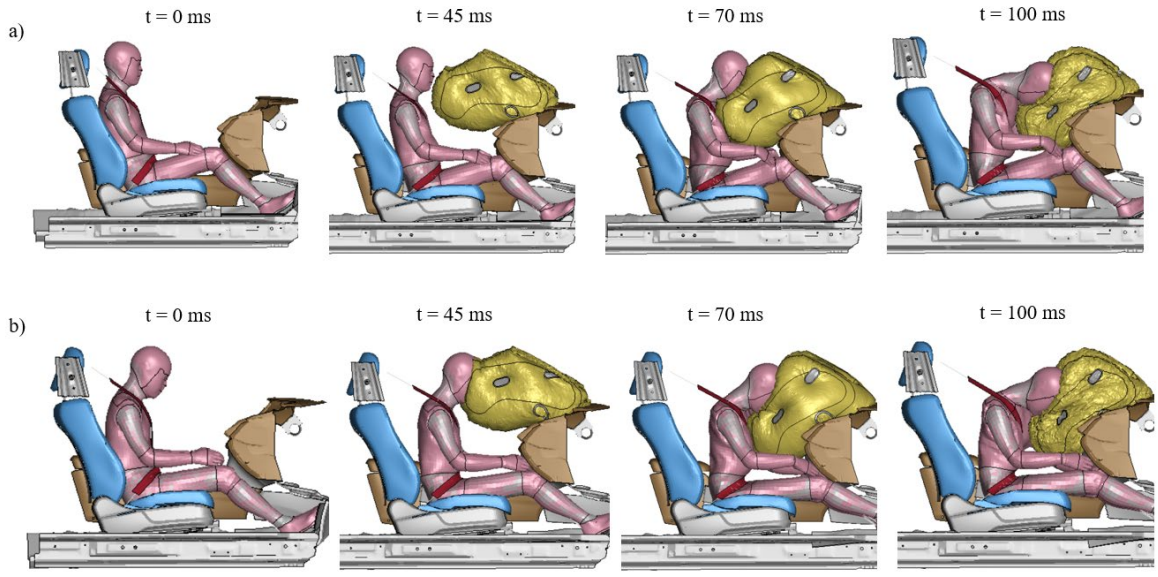

Figure 52. Right view during full frontal crash (56 kmph) with GHBMCsi-M50 (a) without pre-crash - standard position, (b) with pre-crash phase at t =0ms, t=45ms, t=70ms, and t=100ms

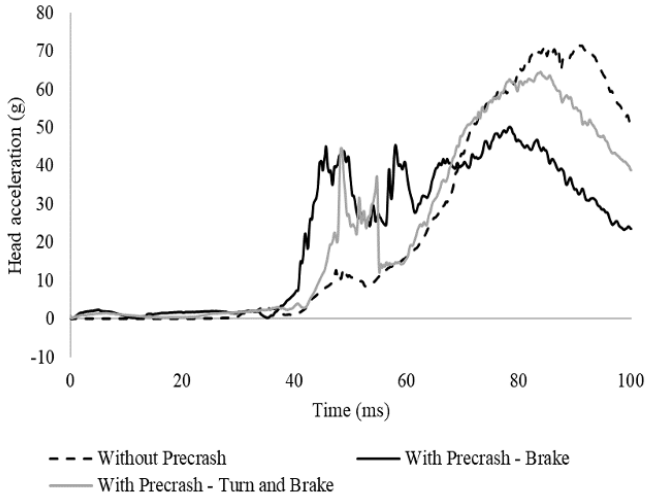

Figure 53. Comparison of head accelerations for different crash scenarios using the GHBMC-M50

The values of injury metrics were extracted from FE simulations and then used to calculate the probability of serious (AIS 3+) injuries for different body regions. As the results show (Table 11), the highest injury risk (6.4%) was recorded for the head during the simulation without a pre-crash maneuver. This could be caused by the higher head velocity relative to the buck at the time of impact with the PAB (4.86 m/s without pre-crash versus 0.95 m/s with brake pre-crash). The Viscous Criterion (VC) was considered in these simulations but found insignificant in all results and therefore omitted from further presentation/discussion.

Table 11. Injury metrics comparison of GHBMCsi-M50 in different scenarios

Crash Scenario	**Injury Metrics**				
	HIC_{15}	**BrIC**	**N_{ij}**	**Chest Deflection**	**Femur Force (N)**
Without Pre-crash	559	0.58	0.43	58	2696
With Pre-crash - Brake	208	0.52	0.23	41	1724
With Pre-crash - Turn and Brake	431	0.52	0.36	57	1947

The simulation without the pre-crash had the highest chest deflection and the case with the pre-crash braking had the lowest chest deflection (Figure 54a). Also note that the chest deflection during the pre-crash brake event was almost negligible (~1 mm).

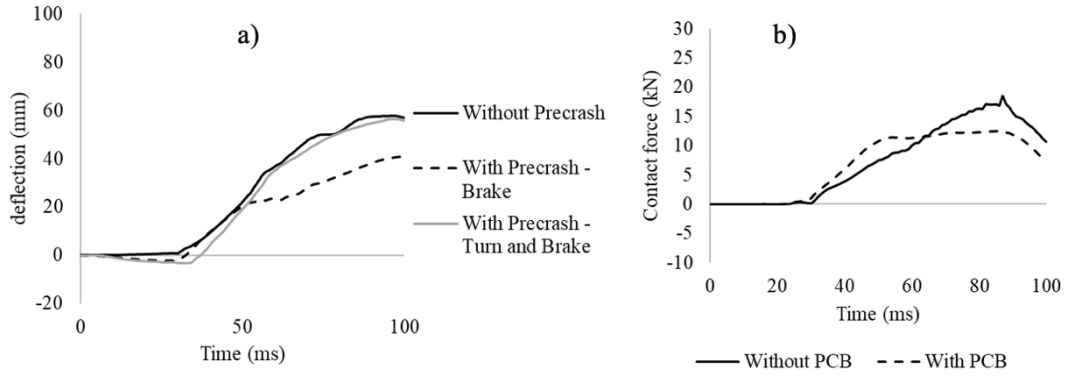

Figure 54. Comparison of (a) chest deflection for different scenarios for GHBMC-M50, (b) resultant belt forces with GHBMCsi

The resultant belt forces with GHBMCsi-M50 for the cases without pre-crash and "with pre-crash brake" are compared in Figure 54b. During pre-crash braking, the belt was already in tension and the belt forces rose steeply and early compared to the case without pre-crash. But since the passenger's upper-body hits the air bag much earlier for the with pre-crash condition, the forward excursion was hindered, causing the belt forces to stagnate and eventually fall. However, for the case without pre-crash, the air bag was contacted much later, and the belt forces kept rising until most of the kinetic energy was transferred to the restraint systems (seat belts and air bag), eventually causing the belt forces to drop.

The injury trends were like what was observed in the literature by Yamada et al. (2016), who also reported higher injury risk when the collision started from the standard position (without pre-crash). As the pre-crash posture and kinematics were introduced into the system, the injury risk was significantly reduced. Similar trends were observed in the different-sized occupants.

Female 5th Percentile (age 20, BMI 25)

Like the FE simulations with the 50th male simplified model discussed in the previous section, the 5th percentile female was positioned using the same seat characteristics, and the same frontal crash simulations were conducted. Then, as shown in Table 12, model responses were compared for three crash scenarios—one starting from standard position, and the others starting with two pre-crash maneuvers of brake and turn-and-brake, to better understand the influence of including the pre-crash phase.

The occupant risk of serious injuries (AIS 3+) was estimated based on HIC15, BrIC, Nij, chest compression, and femur force of the female 5th percentile GHBMCsi model (Table 12). Similar trends were observed in the injury calculations as observed in the male 50th percentile calculations. With the transfer of posture and velocities/kinematics obtained from pre-crash maneuvers, the HIC and femur force values decreased compared to the case without a pre-crash maneuver, showing the significance of kinematics obtained from the pre-crash.

Table 12. Injury metrics comparison of GHBMCsi-F05 in different scenarios

Crash Scenario	Injury Metrics				
	HIC_{15}	BrIC	N_{ij}	Chest Deflection	Femur Force (N)
Without Pre-Crash	514	0.71	0.34	56	1591
With Pre-Crash - Brake	273	0.59	0.20	50	1217
With Pre-Crash – Turn-and-Brake	503	0.63	0.29	53	1355

During the turn-and-brake event, lateral momentum and rotational velocities developed due to the turning maneuver. These played a significant role in the injury calculations, as there was lateral motion of the human body parts during the pre-crash turning and braking, thus adding to injury severity. All body regions incurred higher injury probabilities in the case "with pre-crash turn-and-brake" compared to the case "with pre-crash brake."

Male 95th Percentile (age 20, BMI 25)

FE simulations with the 95th percentile male simplified model were performed and compared for the same three crash scenarios. The results are shown in Table 13. With the transfer of velocities/kinematics, the HIC, BrIC, Nij, chest deflection, and femur force values decreased, as seen in the case with pre-crash braking. This is because the addition of relative velocities between the GHBMC, vehicle, and the restraints play a crucial rule in the collision.

Table 13. Injury metrics comparison of GHBMCsi-M95 in different scenarios

Crash Scenario	Injury Metrics				
	HIC_{15}	BrIC	N_{ij}	Chest Deflection	Femur Force (N)
Without Pre-crash	567	0.56	0.48	81	3641
With Pre-Crash - Brake	458	0.49	0.32	63	1957
With Pre-Crash - Turn and Brake	399	0.45	0.28	55	5277

Interaction With Restraint Systems

Passenger seat occupant safety relies on the seat belt and frontal air bag restraints. The contact forces between occupant-seat belt and occupant-air bag are compared in Figure 55 for the cases with pre-crash braking and without pre-crash braking for the GHBMCsi-M50, F05, and M95 (age 20, BMI 25) to study the influence of pre-crash posture and kinematics.

It was observed that seat belt contact forces were higher for cases without pre-crash braking as compared to cases with pre-crash braking. This may be caused by the GHBMCsi's forward movement towards the dashboard during pre-crash braking. Hence the air bag was contacted much earlier with pre-crash braking, leading to kinetic energy being distributed to the seat belt and air bag. This would lead to smaller seat belt contact forces and larger air bag contact forces, as seen in Figure 55. Whereas in the case without pre-crash braking, most of the kinetic energy was initially captured by the seat belt, leading to larger seat belt contact forces and smaller air bag contact forces.

Similar trends for the driver were reported in the literature (Yamada et al., 2016), considering cases with and without AEB.

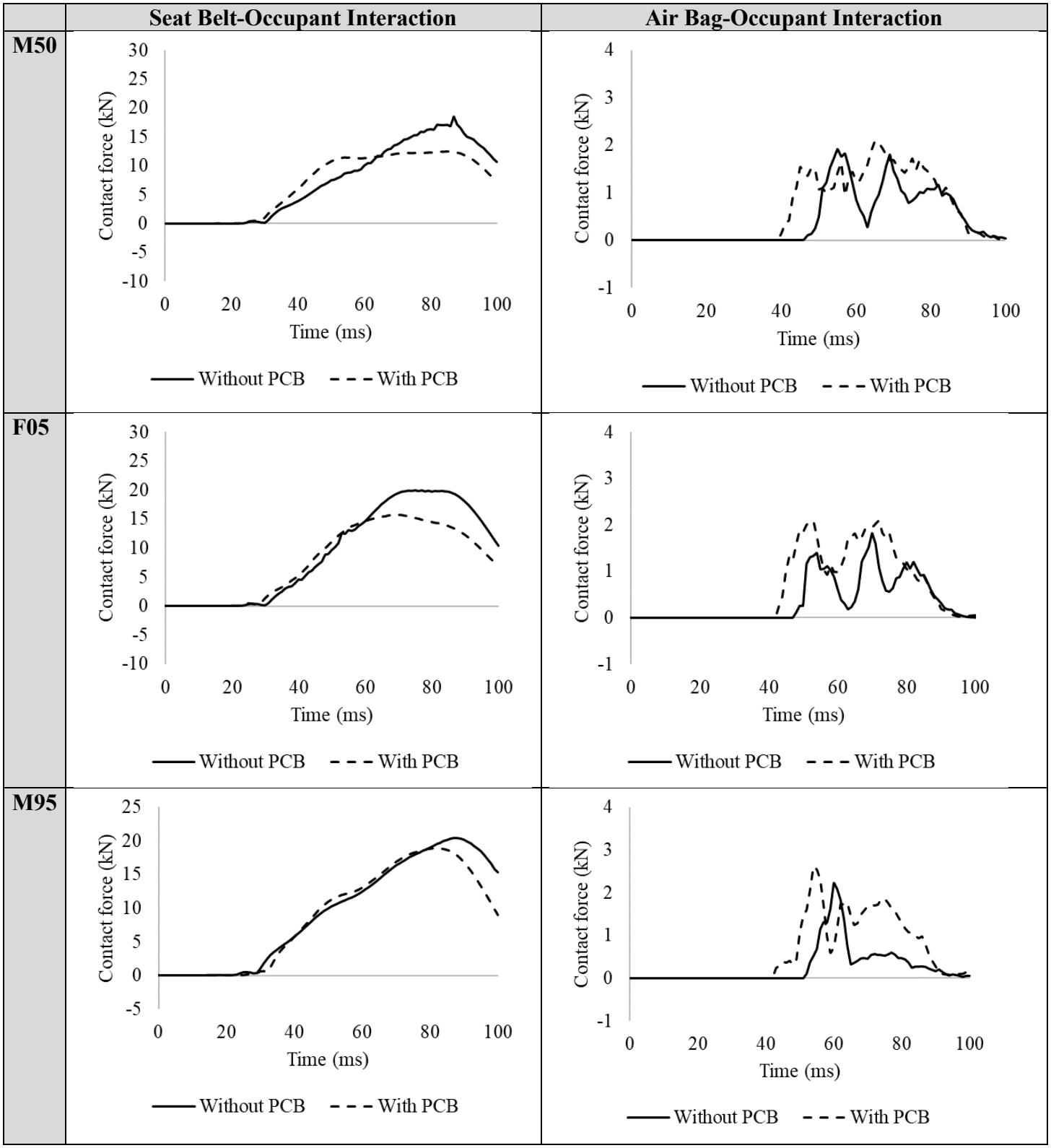

Figure 55. The contact forces between occupant-air bag and occupant-seat belt with GHBMCsi-M50, F05, and M95 (age 20, BMI 25) to study the influence of pre-crash posture and kinematics

A general trend was observed for GHBMCsi's with different size (Fig. 7-5) (age 20, BMI 25), where the risk of injuries in the simulations without pre-crash braking was lower than the simulations with pre-crash braking.

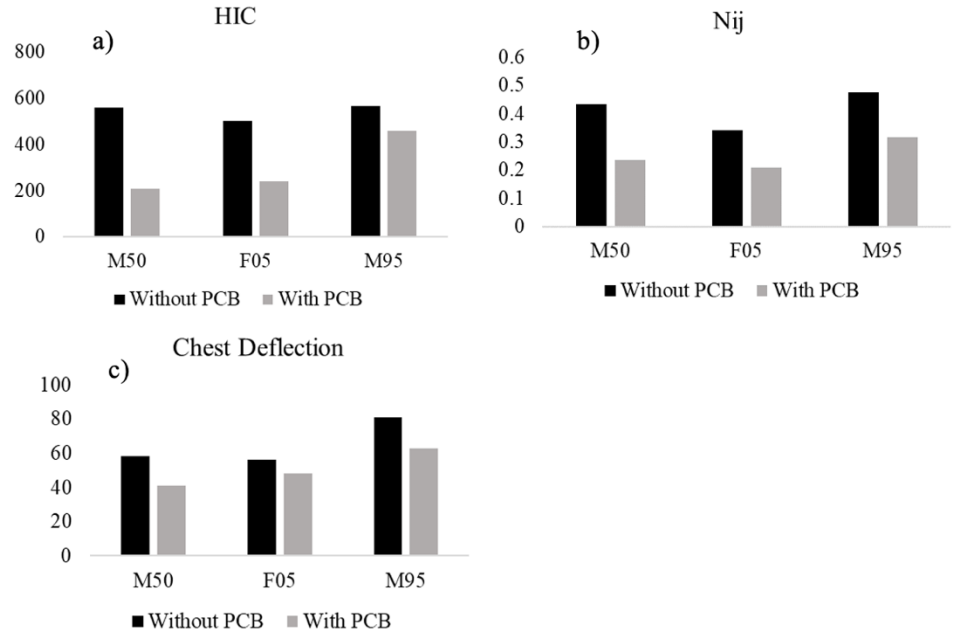

Figure 56. Comparison of head, neck, and chest injuries for the cases with pre-crash braking and without pre-crash braking for the GHBMCsi-M50, F05, and M95 (age 20, BMI 25) to study the influence of pre-crash posture and kinematics

Effect of Seat Track Position

In this subsection, a closer look is taken at the influence of seat track position. Two FE simulations were conducted and compared in a frontal collision with the 5th percentile female simplified model seated in the nominal position (cushion/back seat angles = 0) and the track position close to and away from the dashboard, respectively (Figure 57).

The occupant-air bag and occupant-seat belt contact forces for two seat track levels with the GHBMCsi-F05 were compared (Figure 58). When the GHBMCsi-F05 was seated closer to the dashboard, the air bag hit the ATD earlier and slowed it down, leading to smaller belt forces and larger air bag forces. However, higher belt forces were observed when the GHBMCsi-F05 was seated away from the dashboard (backward seat track position), as the air bag interaction was delayed because of the increased space.

A comparison of injury metrics for level 0 and level 1 seat track positions is presented for GHBMCsi-F05 (Table 14). As expected, higher injury risks for head, brain, neck, and thorax were predicted when the ATD's knee was close to the dashboard (level 0) compared to away from the dashboard (level 1).

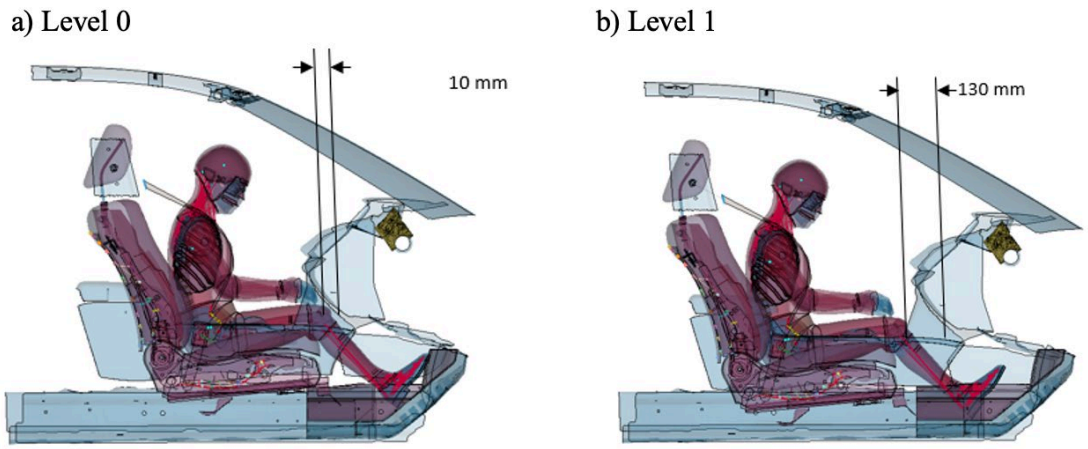

Figure 57. Seat track with GHBMCsi-F05 in the passenger seat at (a) level 0 (knee ~ 10 mm from the dashbord) and (b) level 1 (knee ~ 130 mm from the dashbord), respectively

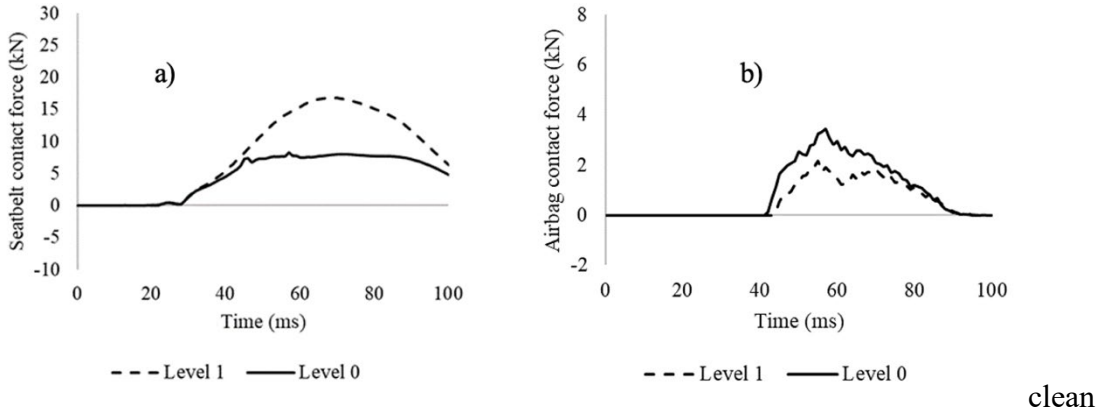

clean

Figure 58. The contact forces were compared for two seat track levels with GHBMCsi-F05 (a) occupant seat belt respectively and (b) between occupant air bag

Table 14. Injury metrics comparison of GHBMCsi-F05 for different seat track levels

Crash Scenario	**Injury Metrics**				
	HIC_{15}	**BrIC**	**N_{ij}**	**Chest Deflection (mm)**	**Femur Force (N)**
Level 0	228	0.58	0.33	32	1907
Level 1	237	0.72	0.37	47	1444

Injury Metrics and Assessed Injury Probabilities From Design-of-Experiment Simulations

The aim of this subsection is to discuss and analyze the injury risks for the design-of-experiment study. An analysis of variance (ANOVA) and global sensitivity analysis (Figure 59, Figure 60) of the design-of-experiment variables were performed using LS-OPT v7.0.

BrIC was most sensitive to HBM size, pre-crash maneuver type, and seat track position (Figure 59a). HIC was most sensitive to seat recline angle and seat track position (Figure 59b). Both seat characteristics changed the position of the head significantly with respect to the air bag. This influenced the interaction timing and duration of the head impact with the passenger air bag.

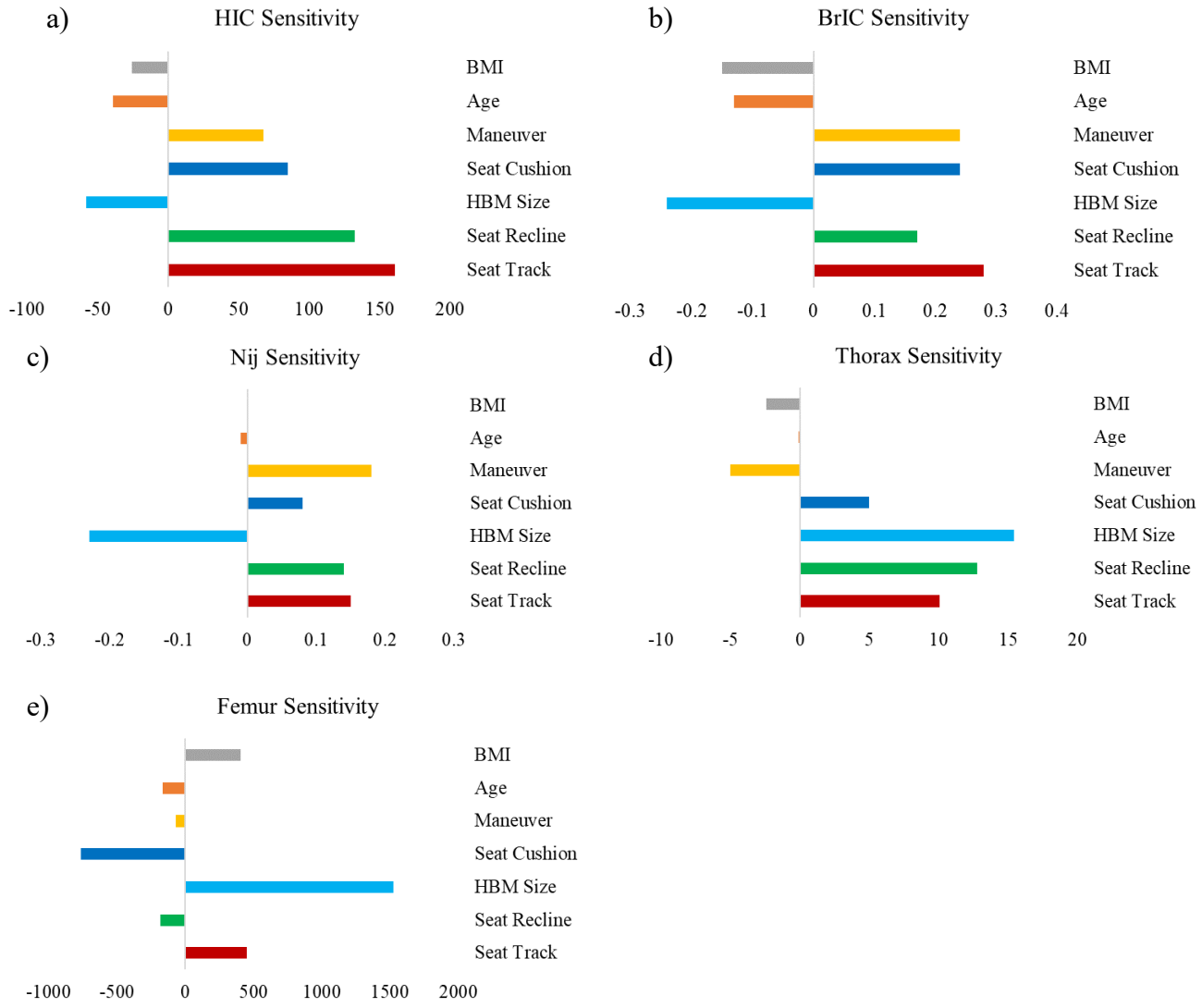

Figure 59. Sensitivities plot for (a) HIC 15, (b) BrIC, (c) Nij, (d) thorax (chest deflection), and (e) femur force

Nij was most sensitive to pre-crash maneuver type and HBM size (Figure 59c). The lateral momentum during turn-and-brake influenced Nij significantly. Seat characteristics also majorly influenced the interaction timing and duration of the head impact with the passenger air bag; hence, farther seat track position, seat back angle, and seat cushion angle led to higher neck injury risks.

Seat recline angle and HBM size greatly influenced the chest/thorax deflections (Figure 59d). Higher recline angles led to delayed interaction with the air bag, causing the shoulder belt to

absorb all the momentum. This in turn resulted in higher chest deflections and larger thoracic injury risk.

The seat track position and seat recline angle showed the highest influence on head injuries. (Figure 60). The brain was the most sensitive to the pre-crash maneuver and the location of the seat track. The neck was quite sensitive to the type of maneuver and the seat recline angle. The thorax was sensitive to HBM size. The abdomen injury risks were minor, but they were most sensitive to HBM size and pre-crash maneuver type.

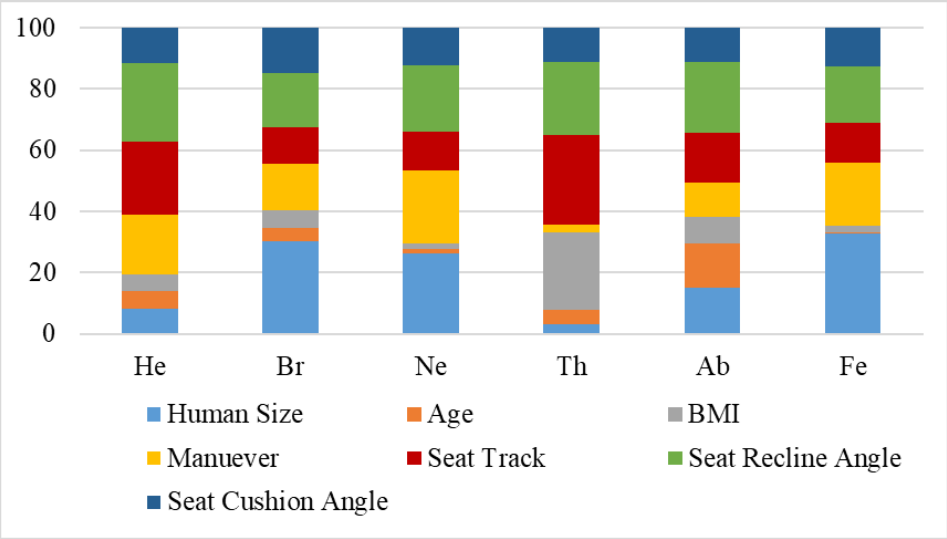

Figure 60. Global sensitivity analysis for all the considered parameters in the design-of-experiment study with respect to various body region injuries including He (head), Br (brain), Ne (neck), Th (thorax), Ab (Abdomen), and Fe (femur)

This page is intentionally left blank.

Study Limitations

Limitations of this study include:

- The muscle activation effects in the pre-crash models were calibrated using optimization only in terms of the time histories of head excursion, and no other body region excursions were considered during the CORA score-based optimization.
- The developed switching algorithm only considered the HBM's posture and kinematics, including the nodal location and velocities of the vehicle, but did not transfer the stress/strain data from the pre-crash phase to in-crash phase.
- During the study, 12 different GHBMCsi-pre models (for the pre-crash phase) and GHBMCsi models (for the in-crash phase) depicting different anthropometry, age, sex, and BMI were simulated. It should be mentioned that although the "young" and "old" GHBMC models had different geometries, they shared the same material properties.
- The study was limited to belted front passengers.
- The statistical results from the parametric study depended on the chosen ranges of the variables (and the design-of-experiment scheme).

This page is intentionally left blank.

Concluding Remarks

By employing a rigid-body GHBMCsi-pre model during a pre-crash phase and a deformable simplified GHBMCsi model during an in-crash phase, high computational costs of running long pre-crash simulations were avoided. Muscle activation was simulated using joint activation in the almost rigid body pre-crash model (GHBMCsi-pre), and the level of activation was calibrated against volunteer test data recorded during pre-crash maneuvers. A switch algorithm was developed to ensure successful and efficient position and kinematic transfer to a deformable simplified GHBMCsi (in-crash) model. Improvements in the overall 2014 Honda Accord FE model PAB deployment were performed, and a robust and symmetric PAB deployment was achieved. A series of PAB validations during frontal and oblique impacts were performed, including a drop tower test to ensure the air bag's performance and stability during different crash scenarios.

The developed switch algorithm was able to effectively integrate both the posture and kinematics of the rigid HBM in the final stage of the pre-crash phase to the corresponding initial conditions of the deformable HBM used to simulate the crash impact. During both pre-crash maneuvers, the occupant's head and thorax moved forward towards the dashboard. Therefore, the head and thorax contacted the PAB earlier, leading to lower head accelerations when the pre-crash phase was considered. In the simulation without any pre-crash maneuvers, the maximum forward displacement of the thorax in the frontal collision was higher, leading to higher chest deflection. In general, lower injury values were observed when pre-crash maneuvers were considered for in-position occupants. A similar trend has been observed for drivers in the literature. Higher injury values were observed for pre-crash turning and braking compared to pre-crash braking due to the lateral momentum gained during turning.

By simulating frontal crashes for two different pre-crash maneuvers, it may be concluded that the severity of injury sustained by a belted passenger decreased for the cases when the pre-crash phase was simulated. This could be explained mostly due to the lower velocity difference between the occupant (e.g., head) and restraint system (e.g., air bag) in the initial phase of a crash. A total of 55 design-of-experiment simulations were performed and injury metrics were recorded for all the belted GHBMCsi models to evaluate passenger injury risks. Seat recline angle and seat track position showed the highest influence on HIC. BrIC and Nij were most sensitive to pre-crash maneuver type, seat recline angle, and HBM size.

Finally, it should be mentioned that the conclusions of the current study are referring to belted passengers. A recent study based on known restraint use (NHTSA, 2023) reported that fifty percent of passenger vehicle occupants killed in traffic crashes in 2021 were unrestrained.

References

Antona, J., Ejima, S., & Zama, Y. (2011). Influence of the driver conditions on the injury outcome in front impact collisions. *International Journal of Automotive Engineering*, *2*(2), 33-38.

Bose, D., Crandall, J. R., Untaroiu, C. D., & Maslen, E. H. (2010). Influence of pre-collision occupant parameters on injury outcome in a frontal collision. *Accident Analysis and Prevention*, *42*(4), 1398-1407.

Carlsson, S., & Davidsson, J. (2011, September 14-16). *Volunteer occupant kinematics during driver initiated and autonomous braking when driving in real traffic environments*. 2011 International IRCOBI Conference, Krakow, Poland.

Chiu, K. A. (2012, November 7). New Car Assessment Program (NCAP) frontal barrier impact test, Honda of America Mfg., Inc, 2013 Honda Accord EX-L 4-door sedan (NHTSA Test No. MD5303. Report No. NCAP-KAR-13-021). National Highway Traffic Safety Administration. https://nrd-static.nhtsa.dot.gov/reports/vehdb/v00000/v08000/v08035R001.pdf

Ejima, S., Zama, Y., & Ono, K. (2009, June 15). *Prediction of pre-impact occupant kinematic behavior based on the muscle activity during frontal collision*. 21st International Technical Conference on the Enhanced Safety of Vehicles, Stuttgart, Germany.

Gennarelli, T. A., Wodzin, E., & Association for the Advancement of Automotive Medicine. (2008). *Abbreviated Injury Scale 2005 update 2008*.

Ghosh, P., Andersson, M., Vazquez, M. M., Svensson, M., Mayer, C., & Wismans, J. (2015, September 9-11). *A proposal for integrating pre-crash vehicle dynamics into occupant injury protection evaluation of small electric vehicles*. 2015 International IRCOBI Conference, Lyon, France.

Hu, J., Lin, Y., S,, Boyle, K., & Reed, M. (in press). *Parametric model for simulating occupant responses during pre-crash vehicle maneuvers*. National Highway Traffic Safety Administration.

Hu, J., Zhang, K., Reed, M. P., Wang, J.-T., Neal, M., & Lin, C.-H. (2019). Frontal crash simulations using parametric human models representing a diverse population. *Traffic Injury Prevention*, *20*, S97-S105. https://doi.org/10.1080/15389588.2019.1581926

Infantes, E., Caspar, M., Kramer, S., & Schaub, S., Langner, T., Eggers, A., Unselt, T., & Lemmen, P. (2015). *The effect of pre-crash safety systems to occupant protection in offset frontal impacts*. (SAE Technical Paper 2015-26-0164). SAE International.

Lebarbé, M., Potier, P., Baudrit, P., Petit, P., Trosseille, X., & Vallancien, G. (2005). Thoracic injury investigation using PMHS in frontal air bag out-of-position situationsns. *Stapp Car Crash Journal*, *49*, 323-342.

Lewandowski, J. (2006, April 3-6). *Federal Motor Vehicle Safety Standard (FMVSS) 208 – occupant crash protection: right front passenger test methodologies*. [Presentation]. SAE 2006 World Congress & Exhibition, Detroit, MI.

Martynenko, O. V., Neininger, F. T., & Schmitt, S. (2019, June 10-13). *Development of a hybrid muscle controller for an active finite element human body model* in LS-DYNA capable of occupant kinematics prediction in frontal and lateral maneuvers. 26th ESV Conference, Eindhoven, the Netherlands.

Meijer, R., van Hassel, E., Broos, J., Elrofai, H., van Rooij, L., & van Hooijdonk, P. (2012, September 12-14). *Development of a multi-body human model that predicts active and passive human behaviour*. 2012 International IRCOBI Conference, Dublin, Ireland.

Montgomery, D. C. (2019). *Design and analysis of experiments*. Wiley.

National Highway Traffic Safety Administration. (2022). *Crash simulation vehicle models*. [Web page and portal]. https://www.nhtsa.gov/crash-simulation-vehicle-models

NHTSA. (2023, May). *Occupant protection in passenger vehicles: 2021 data* (Traffic Safety Facts. Report No. DOT HS 813 449).

Osth, J., Brolin, K., & Bråse, D. (2015). A human body model with active muscles for simulation of pretensioned restraints in autonomous braking interventions. *Traffic Injury Prevention*, *16*, 304-313. https://doi.org/10.1080/15389588.2014.931949

Öztürk, A., Mayer, C., Kumar, G, H., Ghosh, P., Mishra, A., Chitteti, R. K., & Fressmann, D. (2019, June 10-13). *A step towards integrated safety simulation through pre-crash to in-crash data transfer*. 26th ESV Conference, Eindhoven , The Netherlands.

Rawska, K., Gepner, B., Moreau, D., & Kerrigan, J. R. (2020). Submarining sensitivity across varied seat configurations in autonomous driving system environment. *Traffic Injury Prevention*, 1-6. https://doi.org/10.1080/15389588.2020.1791324

Reed, M. P., Ebert, S. M., Jones, M. L. H., & Park, B.-K. (2021). *Occupant dynamics during crash avoidance maneuvers* (Report No. DOT HS 812 997). National Highway Traffic Safety Administration. https://rosap.ntl.bts.gov/view/dot/54737/dot_54737_DS1.pdf

Rooij, L. V. (2011, June 13-16). *Effect of various pre-crash braking strategies on simulated human kinematic response with varying levels of driver attention*. 22nd International Technical Conference on the Enhanced Safety of Vehicles, Washington, DC.

Schwartz, D., Guleyupoglu, B., Koya, B., Stitzel, J. D., & Gayzik, F. S. (2015). Development of a computationally efficient full human body finite element model. *Traffic Injury Prevention*, *16*, S49-S56. https://doi.org/10.1080/15389588.2015.1021418

Singh, H., Ganesan, V., Davies, J., Paramasuwom, M., & L., G. (2018, August). *Vehicle interior and restraints modeling development of full vehicle finite element model including vehicle interior and occupant restraints systems for occupant safety analysis using THOR dummies* (Report No. DOT HS 812 545). National Highway Traffic Safety Administration. https://www.nhtsa.gov/sites/nhtsa.gov/files/documents/812545_edagvehicleinteriorandrestraintsmodelingreport.pdf

Sohr, S., Hofmann, H., Kutschenreuter, S., & Ruck, H. (2007, June 18-21). *Influence of HIII 5% dummy tolerances on positioning and test results in out-of-position load cases according to the FMVSS 208*. 20th International Technical Conference on the Enhanced Safety of Vehicles Conference, Lyon, France.

Stockman, I. (2016). *Safety for children in cars – Focus on three point seatbelts in emergency events.* [Doctoral thesis, Chalmers University].

Yamada, K., Gotoh, M., Kitagawa, Y., & Yasuki, T. (2016, September 14-16). *Simulation of occupant posture change during autonomous emergency braking and occupant kinematics in frontal collision*. 2016 International IRCOBI Conference, Malaga, Spain.

Appendix A: Driver Results

Frontal Impact With Updated PAB – Driver Correlation Results: HIII-M50 Simulation

The frontal simulations were run with the corrected version of the PAB and compared with the results from the previous PAB. Since no changes were made in the driver air bag, the driver head, chest, and pelvis accelerations from current PAB simulations were very much like results from previous PAB, as shown in Figures A-1, A-2, and A-3.

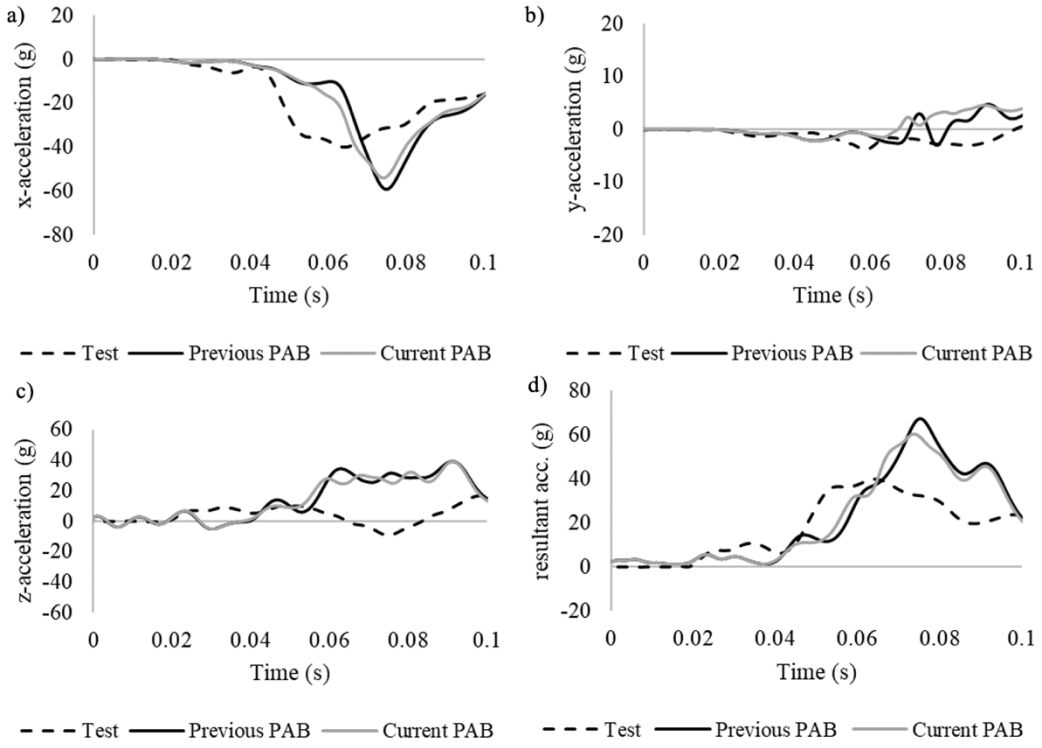

Figure A-1. Comparison of driver's head CG (a) x-acceleration, (b) y-acceleration, (c) z-acceleration, and (d) resultant acceleration

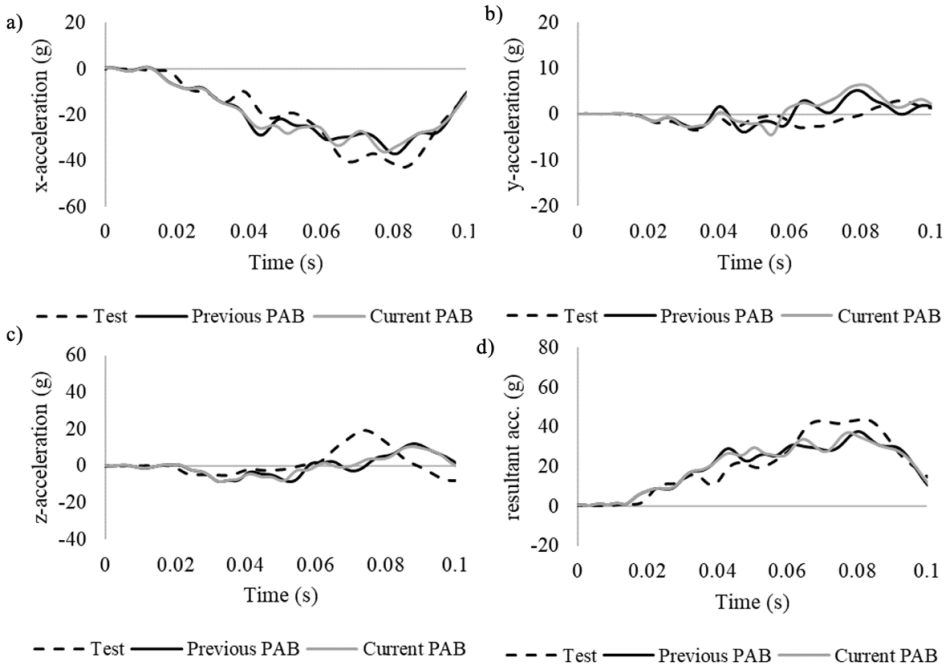

Figure A-2. Comparison of driver's chest CG (a) x-acceleration, (b) y-acceleration, (c) z-acceleration, and (d) resultant acceleration

On the driver's side, no significant differences were observed when using the modified PAB compared to the previous air bag (Figure A-3).

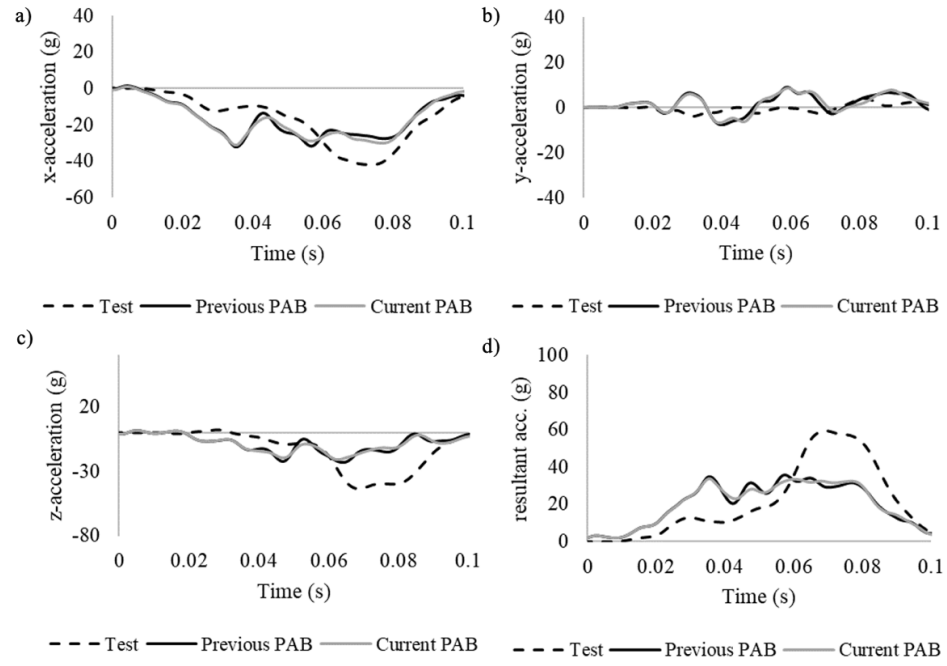

Figure A-3. Comparison of driver's pelvis CG (a) x-acceleration, (b) y-acceleration, (c) z-acceleration, and (d) resultant acceleration

Oblique Impact Left With Updated PAB – Driver Correlation Results: THOR M50 Data

The head and pelvis driver acceleration responses of the THOR M50 ATD recorded during a left oblique crash simulation with the updated PAB model were compared to test data and previous FE data (Figures A-4 and A-5). Since no changes were made in the driver air bag, the driver head and pelvis accelerations from current simulations were very much like the previous results. The overall shape of driver head x-, y-, and z-acceleration showed good correlation, with CORA scores of 0.76, 0.66, and 0.63 respectively. The HIC15 obtained from the current PAB results was at 181 compared to the test at 226.

The THOR's seat belt forces and femur force were also performed as part of the correlation study (Figure A-6). This driver data recorded with the updated PAB were also shown to be almost akin to the corresponding data recorded in the previous FE simulation PAB results.

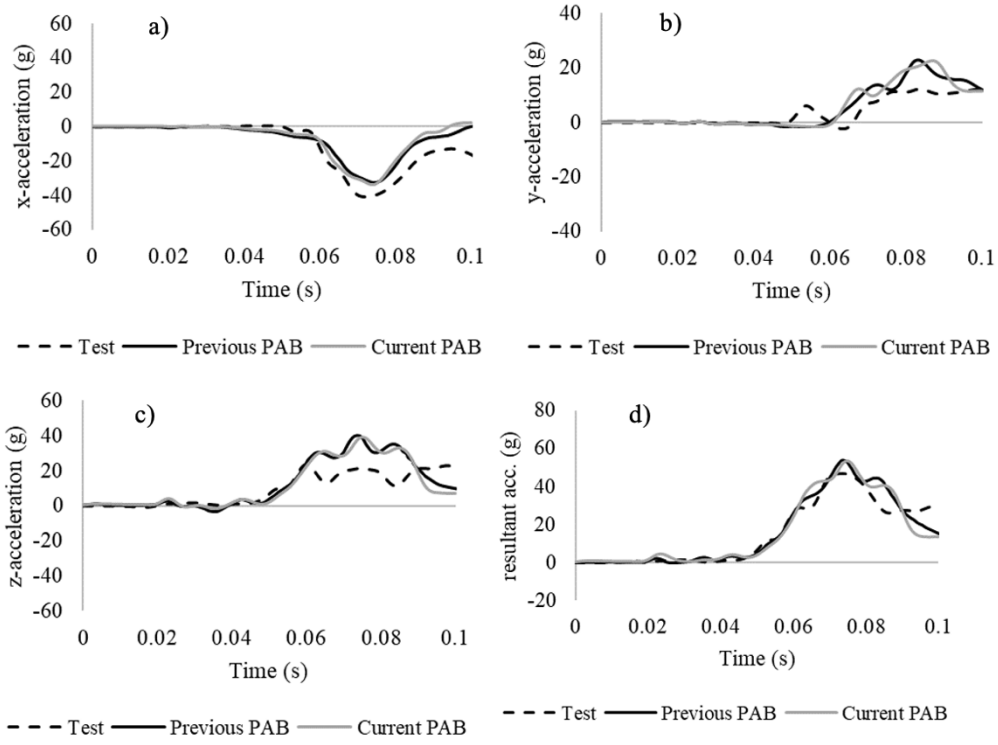

Figure A-4. Driver's head CG (a) x-acceleration, (b) y-acceleration, (c) z-acceleration, and (d) resultant acceleration

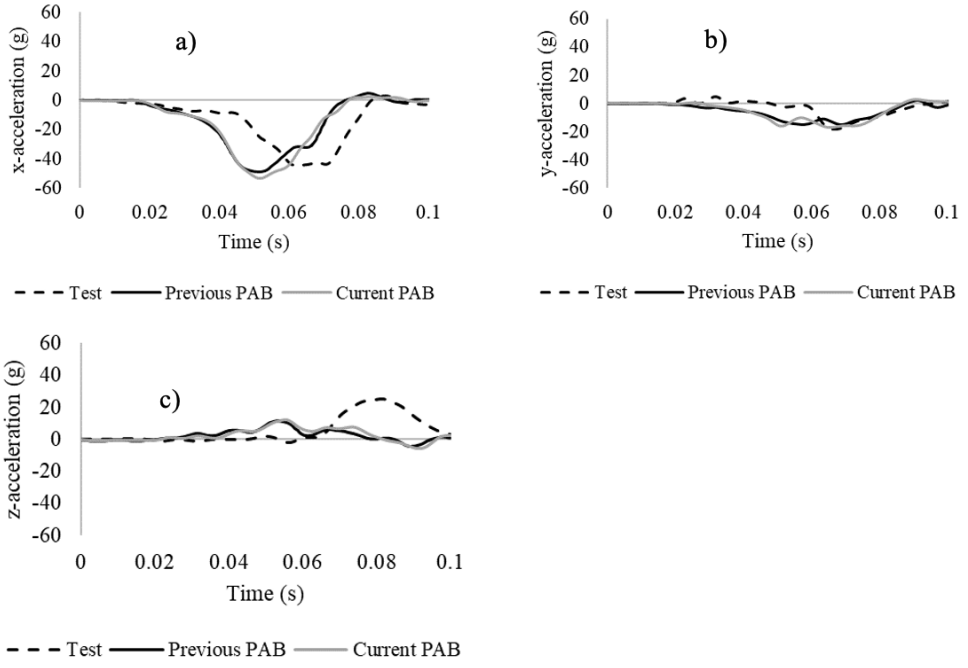

Figure A-5. Driver's pelvis CG (a) x-acceleration, (b) y-acceleration, and (c) z-acceleration

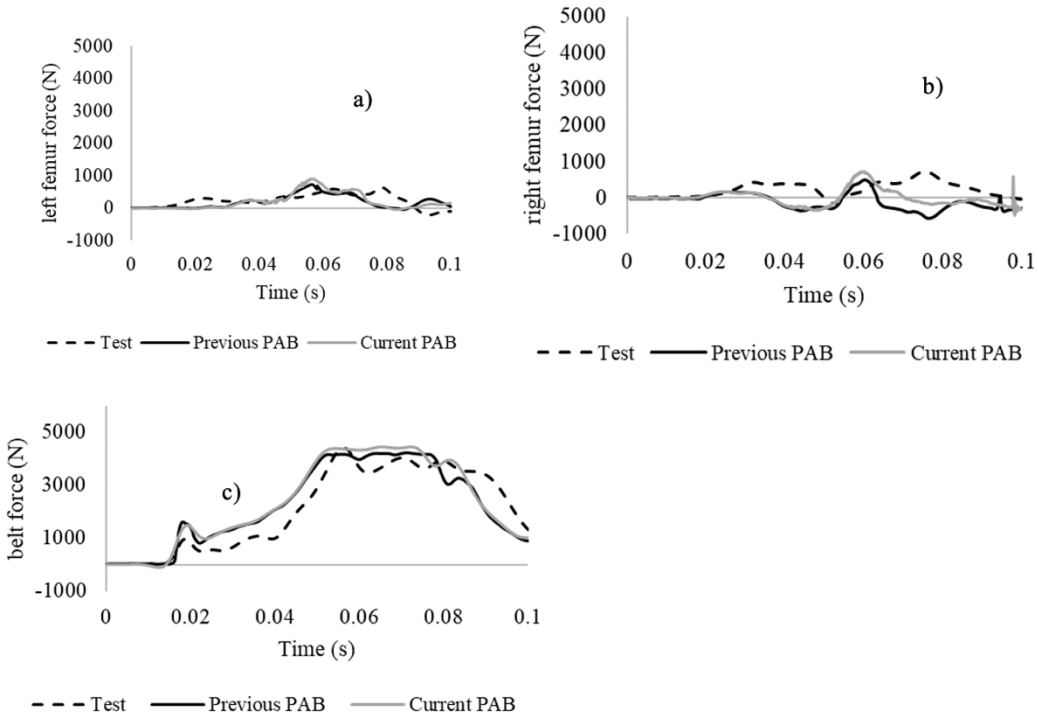

Figure A-6. Comparison of driver's (a) femur left force, (b) femur right force, and (c) upper belt force with results from test, previous PAB, and current PAB

Oblique Impact Right With Updated PAB – Driver Correlation Results: THOR 50M Data

In this subsection, right oblique impact simulations were run with the corrected version of the PAB and the driver results were compared with results obtained using the previous PAB. Since no changes were made in the driver air bag, the driver head, chest, and pelvis accelerations from current PAB simulations were very much like results from the previous PAB as shown in Figures A-7, A-8, and A-9.

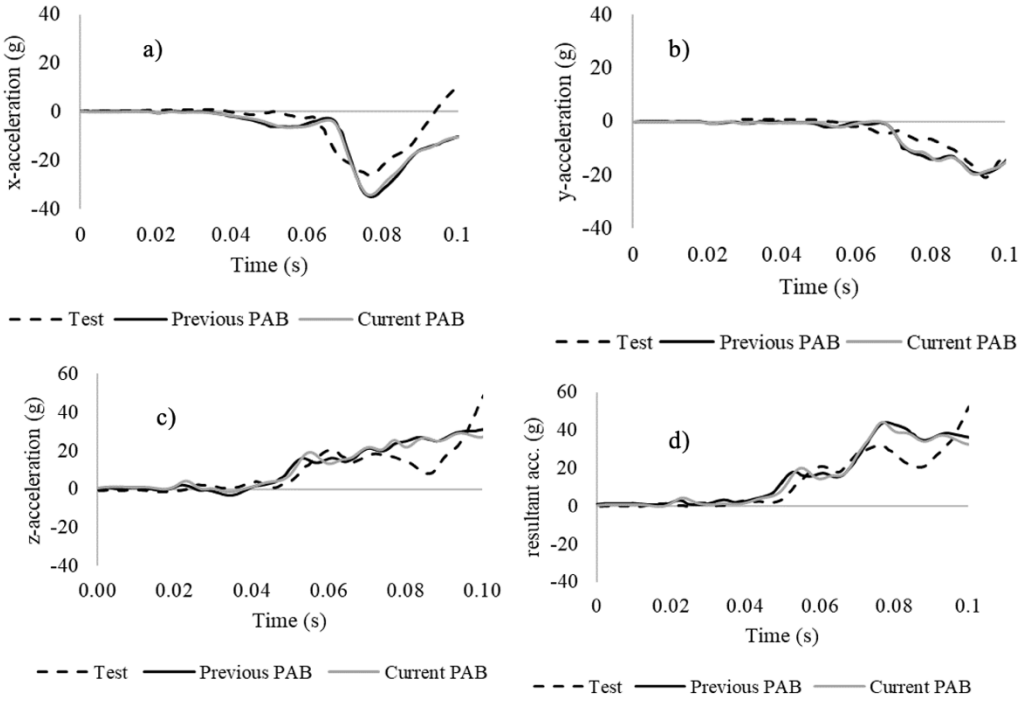

Figure A-7. Comparison of driver's head CG (a) x-acceleration, (b) y-, (c) z-acceleration, and (d) resultant acceleration in right oblique impact

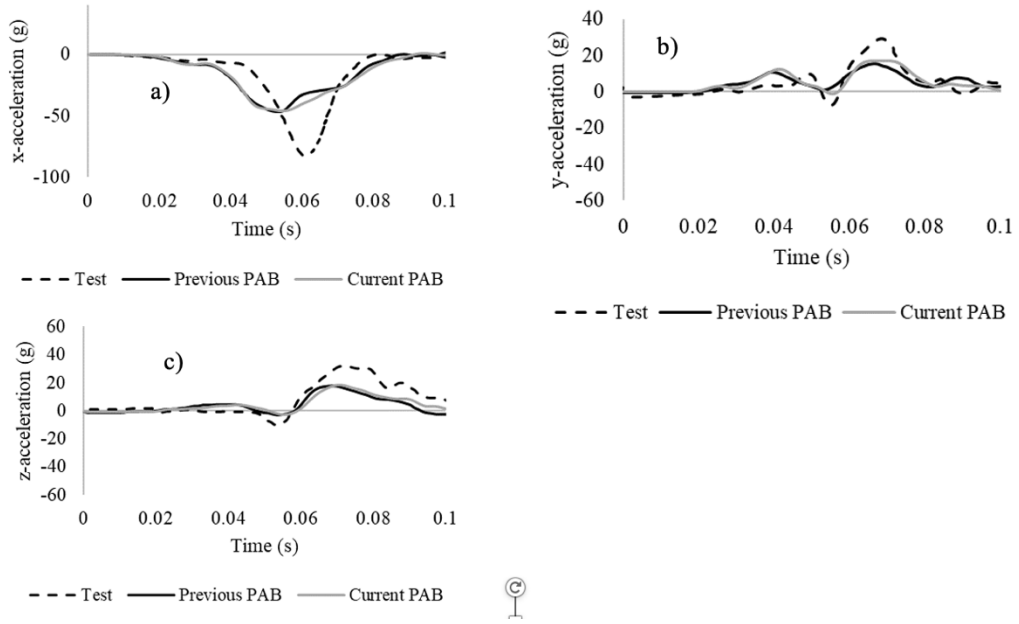

Figure A-8. Comparison of driver's pelvis CG (a) x-acceleration, (b) y-acceleration, and (c) z-acceleration in right oblique impact

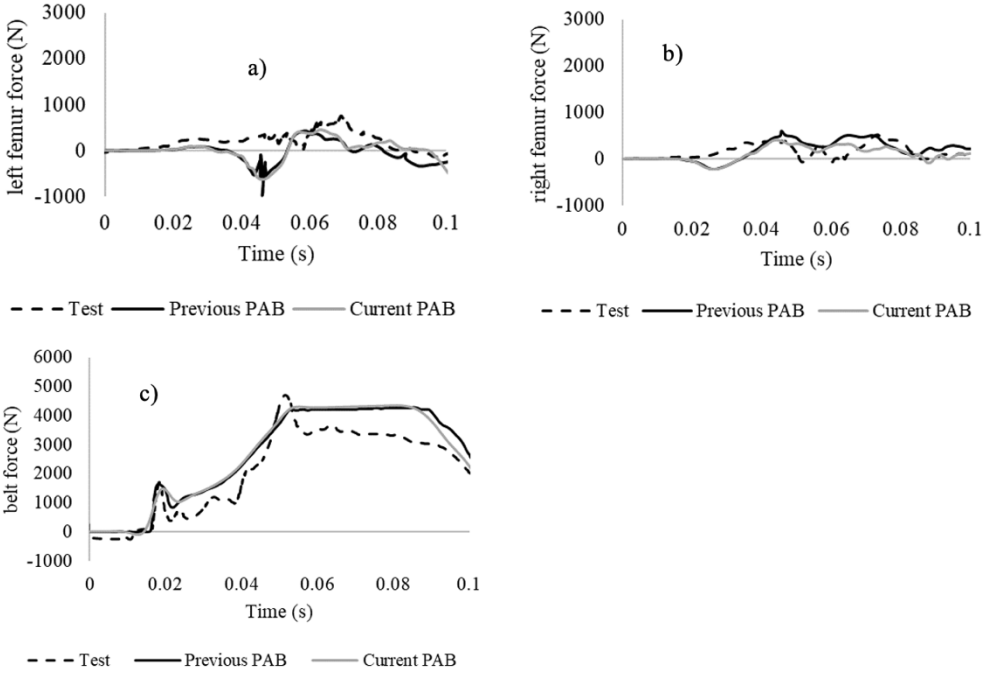

Figure A-9. Comparison of driver's (a) upper belt force, (b) femur left force, and (c) femur right force with results from test, previous PAB, and current PAB in right oblique impact

Appendix B: Issues Faced/Debugged During Design-of-Experiment Simulations

Deformations in the Pelvis Region

During some of the crash simulations, abnormal deformations were observed in the pelvis region in the part: PV_CA_SIJoint_2D. Figure B-1a shows the abnormal deformations in the red sacrum part. The material card was changed to Mooney-Rivlin rubber material as mentioned in Figure B-1b.

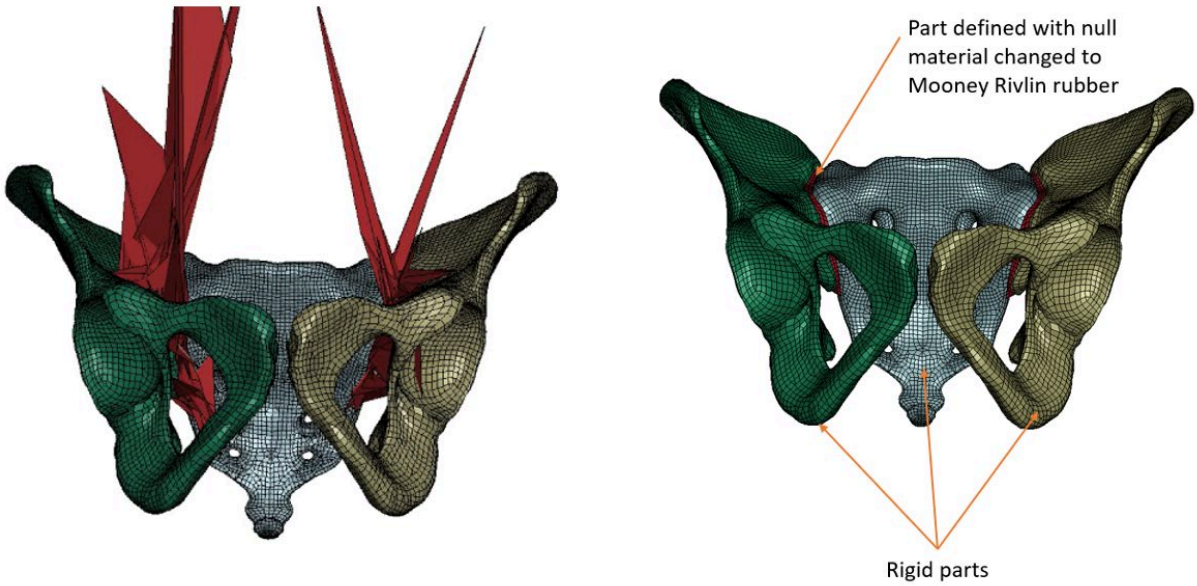

Figure B-1. (a) Deformations observed in red sacrum part in pelvis region. (b) After correcting the material card for the sacrum part to Mooney-Rivlin material

A sacrum part in the pelvis region was updated/corrected as abnormal deformations were observed. The material card related to the part was modified to fix the issue. Some simulations were re-run with the updated sacrum part.

Morphing Issues in BMI 40 GHBMCsi's

Penetrations were observed in the thigh and arm regions after performing the repositioning process for a pre-crash maneuver in obese GHBMCsi's with a BMI of 40. Further morphing was performed using HyperWorks for thigh and arm parts to fix these penetrations (Figure B-2).

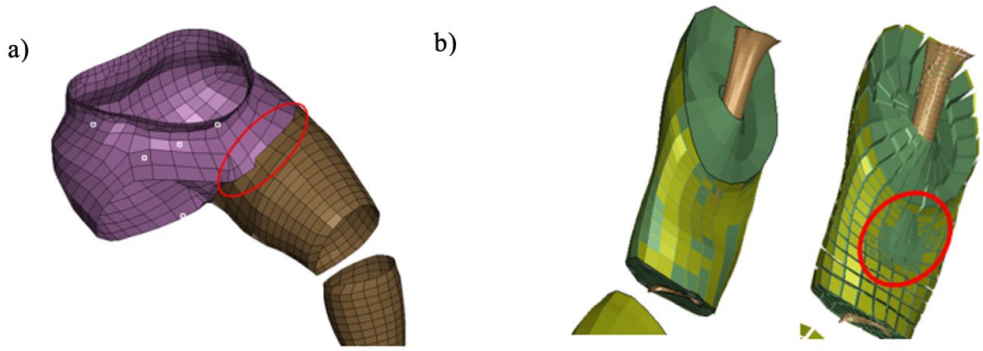

Figure B-2. (a) Penetrations of thigh and pelvis parts (b) Penetrations with arm flesh with bone part

DOT HS 813 631
October 2025

U.S. Department
of Transportation

**National Highway
Traffic Safety
Administration**

16062-092925-v5